Transportation Research Part C 179 (2025) 105279

Contents lists available at ScienceDirect

Transportation Research Part C

journal homepage: www.elsevier.com/locate/trc

Stochastic fundamental diagram modeling of mixed traffic flow: A data-driven approach

Xiaohui Zhang [a,b], Kaidi Yang [b,*], Jie Sun [a], Jian Sun [a,*]

[a] Department of Traffic Engineering & Key Laboratory of Road and Traffic Engineering of Ministry of Education, Tongji University, Shanghai, China

[b] Department of Civil and Environmental Engineering, National University of Singapore, 1 Engineering Drive 2, Singapore, 117576, Singapore

ARTICLE INFO

Dataset link: https://github.com/tjzxh/SFD-modeling-of-mixed-traffic.git

Keywords:
Automated vehicles
Mixed traffic flow
Stochastic fundamental diagram
Mixture density network
Markov chain modeling

ABSTRACT

The integration of automated vehicles (AVs) into existing traffic of human-driven vehicles (HVs) poses significant challenges in modeling and optimizing mixed traffic flow. Existing research on the impacts of AVs often neglects the stochastic nature of traffic flow that gets further complicated by the introduction of AVs, and mainly relies on unrealistic assumptions, such as oversimplified headway or specific car-following (CF) models. The under-utilization of empirical AV datasets further exacerbates these issues, raising concerns about the realism and applicability of existing findings. To address these limitations, this paper presents a novel data-driven framework to model the stochastic fundamental diagram (SFD) of mixed traffic flow using AV trajectory datasets. Specifically, we learn the CF behavior of different leader–follower pairs (HV following AV, HV following HV, AV following HV, AV following AV) from data, unified by a conditional distribution, using the mixture density network (MDN). By formulating the platoon as a joint distribution through Markov chain modeling and incorporating all possible platoon arrangements, we then derive the SFD of mixed traffic flow. Using the NGSIM I-80 dataset, which enables aggregating the empirical fundamental diagram, we validate the proposed framework by demonstrating high consistency with the empirical result. We then apply the framework to the Waymo dataset to evaluate the impact of real-world AVs on traffic flow. The results indicate that larger AV penetration rates lead to decreased mean capacity and critical density while reducing capacity uncertainty, due to the conservative yet stable behavior of current AVs. Overall, this work establishes a general probabilistic modeling framework for mixed traffic flow, enabling the input of real-world AV trajectory datasets and output of the SFD under given AV penetration rates and AV spatial distributions. The proposed framework further facilitates assessing and comparing mixed traffic management strategies, with significant implications for future traffic system design and policy-making.

1. Introduction

The fundamental diagram (FD), characterizing the relationship between macroscopic traffic variables, i.e., flow, density, and speed, has long been a cornerstone of traffic flow theory. In recent years, the stochastic fundamental diagram (SFD) has gained prominence for its capability of capturing the stochastic nature of traffic flow, caused by uncertainties in human driving behavior, dynamic traffic environments, and multiple sources of heterogeneity (Daganzo, 2002; Treiber et al., 2006; Kerner, 2009; Coifman,

* Corresponding authors.
E-mail addresses: tjzxh@tongji.edu.cn (X. Zhang), kaidi.yang@nus.edu.sg (K. Yang), jie_sun@tongji.edu.cn (J. Sun), sunjian@tongji.edu.cn (J. Sun).

https://doi.org/10.1016/j.trc.2025.105279
Received 21 December 2024; Received in revised form 10 July 2025; Accepted 12 July 2025
Available online 25 July 2025

2015). Notably, greater uncertainty is associated with increased traffic instability, often triggering stop-and-go waves and transitions to congestion. Therefore, the SFD also plays a crucial role in developing robust traffic control strategies to mitigate the uncertainty and enhance the stability and overall performance (Keyvan-Ekbatani et al., 2012; Qu et al., 2017; Wang et al., 2021; Zhang et al., 2025).

The importance of SFD modeling has become increasingly evident with the integration of automated vehicles (AVs). First, AV driving behavior tends to be probabilistic and opaque due to the sophisticated artificial intelligence (AI)-based control algorithms (Yu et al., 2021; Zhang et al., 2024), especially in highly automated vehicle systems (i.e. Level 4 and 5). This complicates the modeling of AV-involved traffic flow and necessitates the explicit consideration of the resulting stochasticity. Second, the complex interactions between AVs and human-driven vehicles (HVs) further highlight the need for SFD modeling. Specifically, mixed traffic flow consists of four types of leader–follower pairs: HV following AV (HV-AV), HV following HV (HV-HV), AV following HV (AV-HV), and AV following AV (AV-AV), each exhibiting a different interaction pattern (Hu et al., 2023; Alhariqi et al., 2023). Therefore, the macroscopic properties of mixed traffic flow depend on the platoon arrangements (i.e., permutations of AVs and HVs), which introduce more stochasticity and require rigorous analysis.

Despite the significance of SFD modeling for mixed traffic, existing studies struggle to capture the full stochasticity arising from behavioral uncertainty and diverse platoon arrangements, and primarily focus on estimating the deterministic FD. These studies can be broadly divided into three categories: trajectory data-based, headway-based, and car-following (CF) model-based approaches. Typically assuming a triangular shape, trajectory data-based approaches directly construct the FD via extended Edie's definition with self-collected data of mixed platoons (Shi and Li, 2021). Limited to the self-collected data, these trajectory data-based approaches can hardly be generalized to different conditions to account for stochasticity. Headway-based approaches utilize the inter-vehicle headway, often employing the headway distribution, and its reciprocal relationship to flow rate for FD modeling (Zhou and Zhu, 2020). However, the headway-based approaches oversimplify the complex driving behavior as the headway, and thus fail to capture the correlated microscopic interaction and the uncertainty at this behavioral level. Imposing strong assumptions on the longitudinal behavior, CF model-based approaches utilize specific CF models for each type of pair, and then simulate the FD for mixed platoons (Yao et al., 2023; Jiang et al., 2024b). Even extending these specific CF rules with additional random terms to represent behavioral uncertainty, laborious simulations are required to enumerate all the platoon arrangements exhaustively, which hinders efficient and systematic evaluation. In summary, despite strong assumptions (i.e., the triangular FD shape and specific CF models) or oversimplification (i.e., the headway for driving behavior), few existing approaches are able to effectively model the SFD of mixed traffic, considering both behavioral uncertainty and diverse platoon arrangements.

Beyond their failure to comprehensively account for stochasticity, existing studies rarely utilize open AV datasets. These publicly open data collected by AV companies are typically larger in scale and more widely accepted compared to self-collected data, providing valuable insights into real-world AV operations. Without utilizing these AV datasets, existing studies may not realistically characterize the AV behavior and its impact on traffic (Martínez-Díaz et al., 2024). However, using AV datasets presents several challenges. First, the very few existing AV datasets typically consist of short time segments (e.g., 20 s) sparsely located in AV operating regions (Liu et al., 2024). These fragmented trajectories make it difficult to directly aggregate the FD or calibrate CF models compared to fully observed trajectories in HV datasets. Second, even with complete trajectories, AV datasets would still be constrained to certain conditions with particular penetration rates and spatial distributions, which is challenging to generalize and capture the full spectrum of mixed traffic dynamics. These challenges are substantial obstacles but further underscore the need for empirically grounded SFD research that can effectively adapt to sparse AV trajectory datasets.

To address the aforementioned gaps and challenges, this paper aims to establish a more general SFD modeling framework that captures the stochasticity in mixed traffic arising from the complex AV behavior and diverse platoon arrangements, leveraging AV datasets while adapting to their sparsity. To this end, we develop a data-driven probabilistic framework for SFD modeling of mixed traffic, as shown in Fig. 1. This framework learns microscopic vehicle interactions from empirical trajectory data to ensure realism and adaptability while seamlessly integrating analytical derivations of the SFD from these interactions to achieve structural representation and scalability. Specifically, we begin by modeling the leader–follower interaction with a conditional distribution, which can be learned from data for different types of leader–follower pairs using the mixture density network (MDN). Building upon this microscopic model, we derive the joint distribution through Markov chain modeling, which represents the collective behavior of the platoon. Incorporating all possible platoon arrangements, we obtain the probabilistic macroscopic relation between flow and density under equilibrium conditions (i.e., the SFD).

The contributions of this study are as follows:

- We present a data-driven framework to model the SFD of mixed traffic flow considering both behavioral stochasticity and diverse platoon arrangements, which is adaptable to sparse AV datasets.
- We explicitly account for two types of stochasticity: (1) the stochastic leader–follower interaction of both AVs and HVs, modeled as the conditional distribution of the follower's state given the leader's velocity, and (2) the stochastic arrangements of AVs and HVs in the platoon, quantified by effectively enumerating all possible permutations.
- We systematically derive the SFD of mixed traffic from AV trajectory datasets. We first learn the proposed leader–follower conditional distribution, which is further decomposed into a two-step process, using the mixture density network. We then model the mixed platoon as a Markov chain and naturally derive the SFD under diverse arrangements.
- We thoroughly validate our framework against the empirical FD in the NGSIM I-80 dataset and simulations, and conduct a case study in the Waymo open dataset to assess the SFD of mixed traffic under varying AV penetration rates, spatial distributions, and lane management strategies, which provides valuable insights for AV deployments.

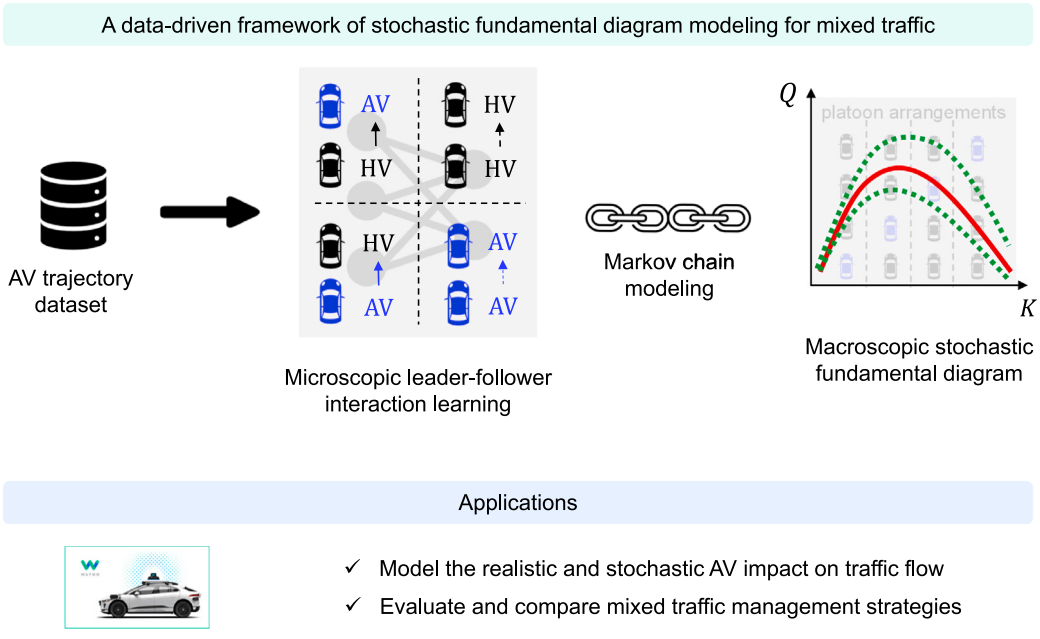

Fig. 1. Overview of this paper.

The rest of the paper is structured as follows: Section 2 reviews the related literature; Section 3 introduces the proposed framework; Section 4 validates the framework with the NGSIM dataset; Section 5 applies the framework to the Waymo dataset as a showcase to estimate the SFD of mixed traffic and evaluate corresponding traffic management strategies; and Section 6 summarizes the main findings.

2. Literature review

2.1. Empirical findings on the AV behavior

Several real-world datasets pertaining to high-level AV systems have been released recently including Lyft Level 5 AV Dataset (Houston et al., 2021), nuScenes Dataset (Caesar et al., 2020), and Waymo Open Dataset (Sun et al., 2020). These AV-oriented datasets collect trajectories of the AV and its surrounding HVs from real-world scenarios, enabling empirical investigations of the AV behavior and its interaction with HV.

The empirical findings on mixed traffic interaction are two-fold. First, there are significant differences between AV and HV driving patterns. Wen et al. (2022) demonstrated that AVs maintain more consistent velocities compared to HVs, leading to enhanced traffic safety and improved behavioral certainty. Moreover, Hu et al. (2023) found that Waymo AVs exhibit a more conservative driving style, prioritizing safety at the expense of efficiency. Second, interestingly, the presence of AVs appears to influence human driving behavior. Many empirical studies report shorter distance and/or time headway for human drivers following AVs than following HVs. Wang et al. (2023) observed that human drivers maintain smaller distances with AVs than HVs in the deceleration process when approaching traffic signals using the Waymo dataset. Furthermore, Jiao et al. (2024) examined the Lyft open data and revealed that the homogeneous driving of AV can be transmitted to the following HV and thus decreases both the variance and the average time headway. Collectively, these empirical findings paint a nuanced picture of different leader–follower interactions in the mixed traffic, where AVs demonstrate more stable yet conservative driving patterns, while human drivers tend to follow AVs more closely.

Nevertheless, it is worth noting that these AV datasets are primarily used for the statistical analysis of microscopic behaviors and are rarely applied in macroscopic studies (see details in the next subsection). The reason lies in that the AV datasets exhibit sparse and discontinuous spatial distributions with short trajectory segments collected from every single AV, which is in contrast with typical HV datasets that offer comprehensive spatial and temporal coverage. This limitation, therefore, poses challenges for applying AV datasets in macroscopic studies of mixed traffic flow.

2.2. Fundamental diagram modeling of mixed traffic flow

There are mainly three approaches for FD modeling of mixed traffic, including trajectory data-based, headway-based, and CF model-based approaches.

Trajectory data-based approaches construct FDs directly from trajectory data, typically collected through self-designed experiments to facilitate macroscopic modeling of mixed traffic. Shi and Li (2021) extended Edie's definition with trajectories from

the CATS Lab and I-75 datasets, and demonstrated the formation of a triangular FD further applied in simulating various mixed traffic scenarios. Using trajectory data collected from multiple experiments of commercial adaptive cruise control (ACC) vehicles under various headway settings, Li et al. (2022b) estimated linear equilibrium spacing-speed relationships for ACC systems, which were then translated into triangular-shaped FDs. By incorporating additional dimensions of traffic state variables and accounting for supply-side factors of roads, Liu et al. (2023) introduced a Gaussian process-based data-driven traffic flow model that extends the classical FD, which is validated through simulation experiments and demonstrates the ability to capture complex relationships between traffic state variables.

Headway-based approaches model the FD from the headway, leveraging its reciprocal relationship with the flow rate. Focusing solely on capacity, Ren et al. (2024) refined the composite headway distribution model by incorporating an automatic iterative algorithm based on extensive empirical data, demonstrating that factors such as penetration rate, platoon intensity, and vehicle type significantly impact mixed traffic capacity. Moreover, Zhao et al. (2024) integrated the stochastic headway model with the autocorrelation-based platooning intensity of CAVs, showing that stronger clustering does not necessarily lead to improved capacity. For the complete flow-density relation, Zhou and Zhu (2020) employed a Gaussian mixture model (GMM) to describe the stochastic headway and then derived the stochastic FD considering CAV penetration rates and platooning intensity in mixed traffic. Guan et al. (2023) developed a tailored Markov chain model to analyze the effects of vehicle platooning, deriving headway type probabilities and simulating FDs in scenarios involving semi- and fully-autonomous vehicles.

CF model-based approaches employ specific CF models for different types of vehicles to simulate the FD of mixed platoon (Martínez-Díaz et al., 2024). Shang and Stern (2021) modeled ACC using the Intelligent Driver Model (IDM), calibrated with data collected from ACC-equipped vehicles, and then examined the impact of ACC on the FD through simulation. Additionally, Jiang et al. (2024b) employed IDM, ACC, and Cooperative Adaptive Cruise Control (CACC) models to simulate different CF modes while considering time lags, platooning intensity and CAV degradation, and obtained the corresponding FD through numerical experiments in mixed traffic. Building upon this CF modeling framework, Wang et al. (2025) examined how dedicated lanes for HVs affect the FD in simulation. Similarly, Lapardhaja et al. (2024) calibrated the CF model in Aimsun to emulate ACC-engaged test cars based on field experiments and then obtained the FD through simulation. Using a frequency-domain representation of vehicle kinematics and a continuum approximation of density and flow, Jiang et al. (2024a) established analytical connections between vehicle dynamics and traffic flow by deriving the dynamic FD directly from CF models.

From the literature review above, we identify three research gaps in the FD modeling of mixed traffic flow. First, the stochasticity stemming from the behavioral uncertainty and platoon arrangements is merely considered, despite being essential for a holistic description and robust control of mixed traffic flow. Second, these studies adopt strong assumptions about the FD model (e.g., the triangular shape) and CF behavior (e.g., specific CF models), or oversimplify the driving behavior using headway. Third, most existing studies lack empirical AV data, potentially resulting in AV behavior inconsistent with reality. To address these limitations, we develop a data-driven framework to derive the SFD of mixed traffic considering the stochastic CF behavior and platoon arrangements, which is effectively applied to the sparse trajectories in AV datasets.

3. Methodology

In this section, we present the general framework to estimate the SFD of mixed traffic flow with AV trajectory datasets. The basic idea is to first learn the microscopic behavior of various leader–follower pairs from sparse AV datasets. Such behavior is modeled as a conditional distribution to capture the dynamics and inherent uncertainty of the interaction between the leader and follower. By linking the leader–follower interaction to the collective behavior of platoon through Markov chain modeling, we then construct the SFD of the mixed platoon incorporating all possible platoon arrangements.

We frame this work as a data-driven framework, while seamlessly integrating analytical derivations, as it fundamentally relies on empirical trajectory data throughout the entire modeling process. By learning microscopic interactions directly from data with the neural network based approach, the framework can capture the realistic interactions in mixed traffic and generalize across diverse behaviors. Aggregating these empirically-derived microscopic behaviors, the analytical derivations of the macroscopic SFD provide a structured representation of traffic dynamics that explicitly characterizes the underlying patterns, ensuring scalability across various platoon configurations.

To avoid ambiguity, we distinguish random variables using upper case letters, including the speed of ith vehicle in the platoon V_i, the spacing between ith vehicle and its leader S_i, the configuration of the platoon arrangement $\boldsymbol{C}$, the equilibrium speed, density and flow of the platoon V, K, Q. Appendix summarizes the notations used throughout this paper.

3.1. Microscopic behavior modeling

3.1.1. Formulation

Stemming from human inconsistency, dynamic environments, and various sources of heterogeneity, driving behavior exhibits inherent uncertainty. Therefore, microscopic states, such as the speed and spacing, are suggested to be modeled as random variables conditioned on its local traffic environment (Branston, 1976; Hoogendoorn and Bovy, 1998; Mahnke and Kaupužs, 1999; Jabari and Liu, 2012; Jabari et al., 2014). To capture this stochastic interaction, we propose the conditional distribution $P(\text{STATES}_i \mid \text{ENV}_i)$, where STATES_i represents the states of vehicle i and ENV_i denotes its surrounding traffic context.

We focus on the CF process, a fundamental behavior that plays a crucial role in shaping the SFD. The widely used assumption in CF modeling, where the follower's state is primarily determined by its leader (Brackstone and McDonald, 1999), is adopted for

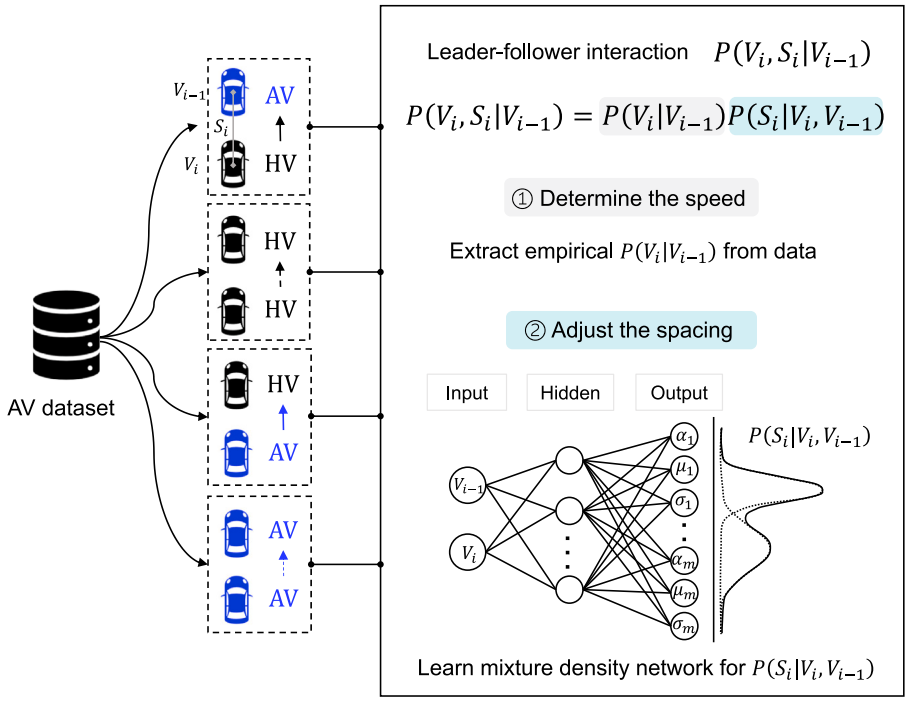

Fig. 2. Stochastic modeling of microscopic behavior for different leader–follower pairs.

both HVs and AVs. Note that this assumption can also be regarded as the Markov property of the CF process. Formally, we define the leader–follower interaction as the conditional distribution of the follower's speed V_i and spacing S_i given the leader's speed V_{i-1}, i.e., $P(V_i, S_i \mid V_{i-1})$, where $P(V_i, S_i \mid V_{i-1}) = P(V_i, S_i \mid V_{i-1}, \dots, V_0, S_{i-1}, \dots, S_1)$. We only model the stationary distribution without considering time evolution, and the transient adaptation process is not explicitly modeled but rather treated as a series of equilibrium states for simplicity and effectiveness. This is reasonable since the SFD under equilibrium mainly depends on stationary conditions. In essence, the proposed leader–follower conditional distribution provides a more general representation of microscopic behavior. Unlike specific CF rules that imply strong assumptions, this conditional distribution naturally captures essential longitudinal interactions while eliminating time evolution, making it both compatible with sparse AV trajectory datasets and effective for modeling macroscopic traffic flow through a joint distribution.

Moreover, this leader–follower conditional distribution can be further decomposed into two parts:

$$P(V_i, S_i \mid V_{i-1}) = \frac{P(V_i, S_i, V_{i-1})}{P(V_{i-1})} = \frac{P(V_i, V_{i-1})}{P(V_{i-1})} \frac{P(V_i, S_i, V_{i-1})}{P(V_i, V_{i-1})} = P(V_i \mid V_{i-1}) P(S_i \mid V_i, V_{i-1}) \tag{1}$$

where we characterize the CF behavior as a two-step process: the follower first decides its speed based on the speed of the leader (represented by the first term $P(V_i \mid V_{i-1})$, assuming that on average the follower's speed is largely driven by the leader's speed, which is supported by the near $y = x$ relationship in scatter plots of follower and leader speeds, see Fig. 4(a)) and then adjusts the spacing between them according to their speeds (represented by the second term $P(S_i \mid V_i, V_{i-1})$). Together, these two parts of the leader–follower interaction determine the state of the follower given the leader's speed.

Reflecting a two-step reaction process, the decomposition further simplifies the learning task. Since the first term can be easily extracted from empirical data, only the second term requires learning. This decomposition allows us to reformulate a one-input, two-output problem ($P(V_i, S_i \mid V_{i-1})$) into a simpler two-input, one-output configuration ($P(S_i \mid V_i, V_{i-1})$). We can thus leverage richer input information for a focused single prediction task, rather than balancing multiple outputs (Caruana, 1997; Bishop, 2006). This two-step modeling framework for microscopic behavior is presented in Fig. 2.

3.1.2. *Learning from data*

Following the two-step formulation of microscopic behavior, for each type of leader–follower pair, we first extract the empirical $P(V_i \mid V_{i-1})$ from dataset by discretizing speeds. Given the natural tendency of the follower to align its speed with the leader (as evidenced in Fig. 4(a)), this simple conditional distribution is nearly uni-modal, making it straightforward to estimate from the data.

The second step of adjusting the spacing given the leader and follower's speeds, $P(S_i \mid V_i, V_{i-1})$, is more challenging. Since it involves an additional dimension and the spacing range is much larger than the speed range, leading to data sparsity under fine-grained discretization, especially given the relatively insufficient data size of AV datasets. Moreover, the spacing varies with the speeds of the leader and follower, and the intricate relationships between these variables are highly likely to result in a multi-modal distribution. Therefore, this complex distribution cannot be estimated accurately through the empirical approach.

To learn this complex conditional distribution $P(S_i \mid V_i, V_{i-1})$ from data, we introduce the mixture density network (MDN). Unlike the Bayesian neural network, which struggles to produce precise and normalized probabilities without costly posterior sampling (Jospin et al., 2022), the MDN integrates conventional neural networks with the mixture density model (e.g., the Gaussian Mixture Model (GMM)) to map the conditional variables to the mixture parameters directly from data, allowing it to approximate any conditional distribution to arbitrary precision (Bishop, 1994). Owing to the flexibility and capability of modeling multi-modal distribution, the MDN is widely applied across diverse fields such as trajectory prediction in robotics (Choi et al., 2018), speech synthesis in acoustic modeling (Zen and Senior, 2014), wind power forecasting in energy management (Zhang et al., 2020) and human pose estimation in computer vision (Li and Lee, 2019). This paper utilizes a commonly used Gaussian mixture model-based MDN to learn the $P(S_i \mid V_i, V_{i-1})$. To ensure a physically meaningful distribution, we further employ the truncated normal distribution (Johnson et al., 2005) to avoid the density leakage problem, as the output spacing is constrained between 0 to a maximum value s_{max}.

Formally, the MDN is a neural network that takes the conditional variables V_i, V_{i-1} as input, and gives the parameters of a Gaussian mixture model as output. In other words, the MDN defines a probability distribution of the output variable S_i conditioned on the input. It follows the form of a Gaussian mixture model given as:

$$P(S_i = s_i \mid V_i = v_i, V_{i-1} = v_{i-1}) = \sum_{m=1}^{M} \alpha_m(v_i, v_{i-1}; \boldsymbol{\theta}) \cdot \mathcal{TN}\left(s_i; \mu_m(v_i, v_{i-1}; \boldsymbol{\theta}), {\sigma_m}^2(v_i, v_{i-1}; \boldsymbol{\theta}), 0, s_{max}\right) \tag{2}$$

where M is the number of mixture components, $\alpha_m(v_i, v_{i-1}; \boldsymbol{\theta})$, $\mu_m(v_i, v_{i-1}; \boldsymbol{\theta})$, and ${\sigma_m}^2(v_i, v_{i-1}; \boldsymbol{\theta})$, respectively, correspond to the mixture weight, mean and variance of the mth truncated normal distribution component $\mathcal{TN}(\cdot)$ given the conditional variables. All these parameters of the mixture model are governed by the neural network with a set of learnable weights $\boldsymbol{\theta}$. For the neural network, we employ a standard multi-layer perceptron, consisting of a single hidden layer with hyperbolic tangent units and an output layer with linear units, as shown below:

$$\alpha_m(v_i, v_{i-1}; \boldsymbol{\theta}) = \frac{\exp\left(z_m^{(\alpha)}(v_i, v_{i-1}; \boldsymbol{\theta})\right)}{\sum_{j=1}^{M} \exp\left(z_j^{(\alpha)}(v_i, v_{i-1}; \boldsymbol{\theta})\right)} \tag{3}$$

$$\mu_m(v_i, v_{i-1}; \boldsymbol{\theta}) = \max\left(0, z_m^{(\mu)}(v_i, v_{i-1}; \boldsymbol{\theta})\right) \tag{4}$$

$$\sigma_m(v_i, v_{i-1}; \boldsymbol{\theta}) = \exp\left(z_m^{(\sigma)}(v_i, v_{i-1}; \boldsymbol{\theta})\right) \tag{5}$$

where $z_m^{(\alpha)}$, $z_m^{(\mu)}$ and $z_m^{(\sigma)}$ are network outputs for the mixture weight, mean and variance of the mth truncated normal distribution component. The use of the softmax function in Eq. (3) constrains the mixture weights to be positive and sum to 1. Similarly, the ReLU (rectified linear unit) function in Eq. (4) and the exponential in Eq. (5) keep the mean and standard deviation positive.

Using maximum likelihood estimation, we train the MDN to find the optimal weights $\boldsymbol{\theta}^*$ of the neural network. Specifically, we minimize the following negative conditional log-likelihood:

$$\boldsymbol{\theta}^* = \arg\min_{\boldsymbol{\theta}} - \sum_{j} \log P_{\boldsymbol{\theta}}(S_i^{(j)} \mid V_i^{(j)}, V_{i-1}^{(j)}) \tag{6}$$

where $D = \left\{\left((V_i^{(j)}, V_{i-1}^{(j)}), S_i^{(j)}\right) \mid j = 1, 2, \ldots\right\}$ is a set of input–output pairs in training data. For the purpose of numerical stability, the adaptive learning rate method Adam (Kingma and Ba, 2014) is employed with gradient clipping technique (Zhang et al., 2019) in the training phase.

3.2. Stochastic fundamental diagram modeling

Based on the proposed microscopic model, in this subsection we derive the SFD of mixed traffic flow incorporating all possible platoon arrangements, see Fig. 3. In particular, we link the proposed leader–follower conditional distribution to the joint distribution of a platoon through Markov chain modeling. By synthesizing all possible platoon arrangements, characterized by configurations that consist of varying compositions of HV-AV, HV-HV, AV-HV and AV-AV pairs, we then obtain the SFD of mixed traffic flow.

3.2.1. Joint distribution of platoon

To capture the collective behavior of the entire platoon for SFD modeling, we aggregate the leader–follower conditional distribution to derive the joint distribution of the platoon. Formally, consider a section of single-lane highway where vehicle i follows vehicle $(i-1)$, as illustrated in Fig. 3, the joint distribution of vehicles' speeds and spacings in the platoon is represented as $P\left(V_1, \ldots, V_n, S_1, \ldots, S_n \mid V_0\right)$, where n is the total number of vehicles in the study section and V_0 is the speed of the leading vehicle in the platoon.

By the chain rule in probability, this joint distribution can be factorized into the product of leader–follower conditional distributions:

$$\begin{aligned} P\left(V_1, \ldots, V_n, S_1, \ldots, S_n \mid V_0\right) &= \prod_{i=1}^{n} P\left(V_i, S_i \mid V_{i-1}, \ldots, V_1, S_{i-1}, \ldots, S_1, V_0\right) \\ &= \prod_{i=1}^{n} P\left(V_i, S_i \mid V_{i-1}\right) \end{aligned} \tag{7}$$

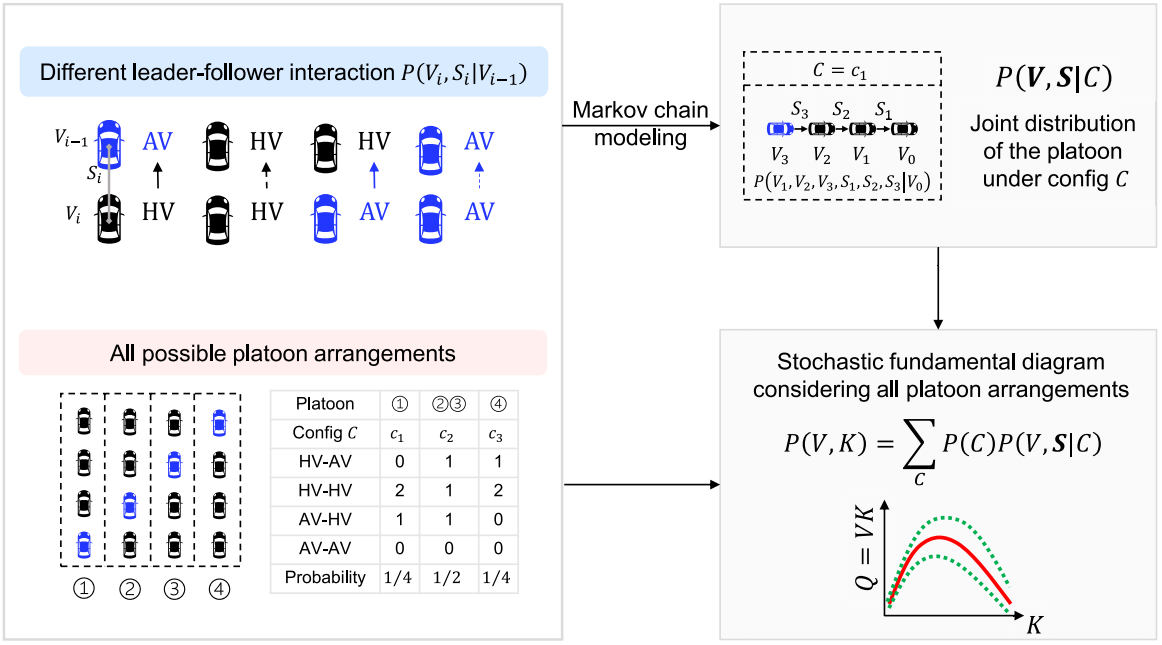

Fig. 3. SFD modeling of mixed traffic flow based on the leader–follower conditional distribution.

where the first equation follows the chain rule in probability, and the second equation results from the adopted Markov assumption for leader–follower interactions, i.e., the speed and spacing of follower i solely depends on the speed of its leader $i-1$.

We further derive the joint distribution of platoon under equilibrium, as the fundamental diagram is the macroscopic relation in equilibrium conditions. In the context of traffic flow, the equilibrium typically implies identical speeds (Treiber and Kesting, 2013; Montanino and Punzo, 2021), denoted by the equilibrium speed V. For a given equilibrium speed $V = v_e$, all vehicles in the platoon adopt this speed value simultaneously, while the corresponding equilibrium spacing can vary due to heterogeneous CF behaviors in the mixed traffic, denoted as $\boldsymbol{S} = (S_1, \ldots, S_n)$. Thus the resulting joint distribution under equilibrium is given as:

$$\begin{aligned} P\left(V = v_e, \boldsymbol{S} = \boldsymbol{s}\right) &= \prod_{i=1}^{n} P\left(V_i = v_e, S_i = s_i \mid V_{i-1} = v_e\right) \\ &= \prod_{i=1}^{n} P(V_i = v_e \mid V_{i-1} = v_e) P(S_i = s_i \mid V_i = v_e, V_{i-1} = v_e) \end{aligned} \tag{8}$$

where the last equation is given by the two-step decomposition in Eq. (1).

3.2.2. SFD derivation incorporating platoon arrangements

The platoon with varying arrangements of AVs and HVs can exhibit different characteristics due to heterogeneous leader–follower interactions, adding another layer of stochasticity to the SFD. To capture the stochastic effects of platoon arrangements, given the total number of vehicles n and AV penetration rate p, we efficiently obtain all unique permutations using lexicographic permutation generation (Sedgewick, 1977). These permutations can be characterized by the composition of pair types, and are thus grouped into platoon configurations denoted as $\boldsymbol{C} = \left(N_{\mathrm{HA}}, N_{\mathrm{HH}}, N_{\mathrm{AH}}, N_{\mathrm{AA}}\right)$, where N_{HA}, N_{HH}, N_{AH} and N_{AA} are the number of HV-AV, HV-HV, AV-HV, and AV-AV pairs respectively. We then calculate the probability of each configuration $P(\boldsymbol{C})$ based on its frequency of occurrence. Here we assume a random spatial distribution of AVs and HVs as the general case, which can be easily replaced with alternative spatial distribution strategies by filtering permutations from the random distribution results based on the desired spatial constraints.

Combining diverse platoon arrangements, characterized by the distribution of platoon configurations, with the dynamics of the platoon under each configuration, represented by the joint distribution, we derive the SFD of the mixed traffic flow under equilibrium. To be specific, given the equilibrium speed v_e, we first obtain the equilibrium joint distribution under each platoon configuration $\boldsymbol{c}$ using Eq. (8):

$$\begin{aligned} P\left(V = v_e, \boldsymbol{S} = \boldsymbol{s} \mid \boldsymbol{C} = \boldsymbol{c}\right) = &\prod_{i=1}^{n_{\mathrm{HA}}} P_{\mathrm{HA}}\left(v_e, s_i \mid v_e\right) \prod_{j=1}^{n_{\mathrm{HH}}} P_{\mathrm{HH}}\left(v_e, s_j \mid v_e\right) \\ &\prod_{m=1}^{n_{\mathrm{AH}}} P_{\mathrm{AH}}\left(v_e, s_m \mid v_e\right) \prod_{r=1}^{n_{\mathrm{AA}}} P_{\mathrm{AA}}\left(v_e, s_r \mid v_e\right) \end{aligned} \tag{9}$$

where $\boldsymbol{c} = \left(n_{\mathrm{HA}}, n_{\mathrm{HH}}, n_{\mathrm{AH}}, n_{\mathrm{AA}}\right)$ is a given platoon configuration, $\boldsymbol{s} = \left(\cdots, s_{n_{\mathrm{HA}}}, \ldots, s_{n_{\mathrm{HH}}}, \ldots, s_{n_{\mathrm{AH}}}, \ldots, s_{n_{\mathrm{AA}}}\right)$ denotes a sequence instance of the corresponding equilibrium spacings in the platoon, and $P_{\mathrm{LF}}\left(V_i, S_i \mid V_{i-1}\right)$ with $\mathrm{LF} \in \{\mathrm{HA}, \mathrm{HH}, \mathrm{AH}, \mathrm{AA}\}$ represents the complete leader–follower conditional distributions.

Using the relation between equilibrium spacing and density $k = \frac{n}{\sum_{i=1}^{n_{\mathrm{HA}}} s_i + \sum_{j=1}^{n_{\mathrm{HH}}} s_j + \sum_{m=1}^{n_{\mathrm{AH}}} s_m + \sum_{r=1}^{n_{\mathrm{AA}}} s_r}$, we have:

$$P\left(V = v_e, K = k \mid \boldsymbol{C} = \boldsymbol{c}\right) = \prod_{i=1}^{n_{\mathrm{HA}}} P_{\mathrm{HA}}\left(v_e, s_i \mid v_e\right) \prod_{j=1}^{n_{\mathrm{HH}}} P_{\mathrm{HH}}\left(v_e, s_j \mid v_e\right) \prod_{m=1}^{n_{\mathrm{AH}}} P_{\mathrm{AH}}\left(v_e, s_m \mid v_e\right) \prod_{r=1}^{n_{\mathrm{AA}}} P_{\mathrm{AA}}\left(v_e, s_r \mid v_e\right) \tag{10}$$

Incorporating all platoon configurations with the law of total probability, we obtain:

$$P\left(V = v_e, K = k\right) = \sum_{\boldsymbol{c}} \underbrace{P\left(V = v_e, K = k \mid \boldsymbol{C} = \boldsymbol{c}\right)}_{\text{stochastic CF behaviors}} \underbrace{P(\boldsymbol{C} = \boldsymbol{c})}_{\text{platoon arrangements}} \tag{11}$$

where this distribution is further normalized to ensure that $\sum_{v_e} \sum_k P\left(V = v_e, K = k\right) = 1$.

Overall, we explicitly capture two key sources of stochasticity: the stochasticity in CF behavior under each platoon configuration and the uncertainty arising from different platoon arrangements, highlighting a core contribution of our work. Note that although the AV penetration rate p does not explicitly appear, it governs the feasible platoon configurations $\boldsymbol{C}$ and their distribution $P(\boldsymbol{C})$.

With $Q = KV$, we further derive the probabilistic relation between flow and density (i.e., the SFD):

$$P\left(Q = kv_e \mid K = k\right) = \frac{P\left(V = v_e, K = k\right)}{P(K = k)} = \frac{P\left(V = v_e, K = k\right)}{\sum_{v_e} P\left(V = v_e, K = k\right)} \tag{12}$$

For each density $K = k$, it gives the distribution of flow Q and allows us to further compute the mean and variance, providing a comprehensive description for macroscopic characteristics of mixed traffic flow.

4. Validation

Due to the lack of ground-truth SFD in sparse AV datasets, in this section, we use the human driving trajectories in the NGSIM I-80 dataset and simulation experiments to validate the proposed framework against the empirical fundamental diagram. Specifically, we seek to demonstrate the capability of our framework to accurately estimate the SFD from sparse trajectory data with short segments. To this end, we first randomly extract 20-s segments from CF events to replicate the sparsity of AV trajectory data, and learn the microscopic model for the leader–follower pair. Incorporating the platoon arrangement, we obtain the estimated SFD that is then verified with the empirical result.

4.1. Validation using NGSIM dataset

4.1.1. Data preparation

We utilize the reconstructed NGSIM I-80 dataset processed by the reconstruction procedure (Montanino and Punzo, 2015) with inconsistencies and noise eliminated. The data were collected along the Interstate freeway I-80 in the San Francisco Bay area during 4:00–4:15 pm on April 13, 2005. There are 6 lanes in the study area, including a left-most High-Occupancy Vehicle (HOV) lane, 4 regular lanes, and a shoulder lane with the on-ramp and off-ramp. In order to avoid abnormal CF states caused by the HOV lane and merging and diverging behaviors, only the trajectory data of automobiles on the central lanes (lane 2, 3, 4) are taken into consideration. To further replicate the sparsity of AV trajectory data, we randomly extract a 20-s segment from each CF pair, leading to a total of 200,090 CF samples for microscopic behavior learning.

We further construct the empirical FD for validation. In particular, we aggregate the trajectory data within lane 2–4 upstream of the on-ramp bottleneck to capture a holistic traffic flow dynamics. The spatial interval for aggregation is 100 m, ranging from 144 m to 244 m of local Y, and the time interval for aggregation is 10 steps (1 s). We then compute the empirical density and flow by Edie's definition (Edie, 1963).

4.1.2. Microscopic behavior learning

Following the proposed two-step model for leader–follower interactions, we first get the empirical speed conditional distribution $P(V_i \mid V_{i-1})$ for the HV-HV pair by discretizing speeds. With a small discretization step, the discretization results (Fig. 4(b)) preserve the main feature of the original data (Fig. 4(a)), where the follower tends to keep a similar speed with its leader as expected.

For the second step, we train the MDN as formulated in Eq. (2), to model the spacing adjustment given the leader and follower's speeds $P(S_i \mid V_i, V_{i-1})$. The hyperparameters are determined by conducting a grid search, and the results are presented in Table 1. Based on these hyperparameters, we then train the MDN with 80% of the extracted CF data. The remaining data is used for testing and is further divided into multiple subsets based on the conditional variables (V_i, V_{i-1}). For each test subset, we calculate the expected spacing of both the trained MDN and the empirical data. The mean absolute error (MAE) and the mean absolute percentage error (MAPE) between these expectations are then used to evaluate the performance of the trained model. The trained MDN achieves a low MAE of 0.62 m and a MAPE of 2.8%, demonstrating its efficacy in replicating microscopic driving behavior.

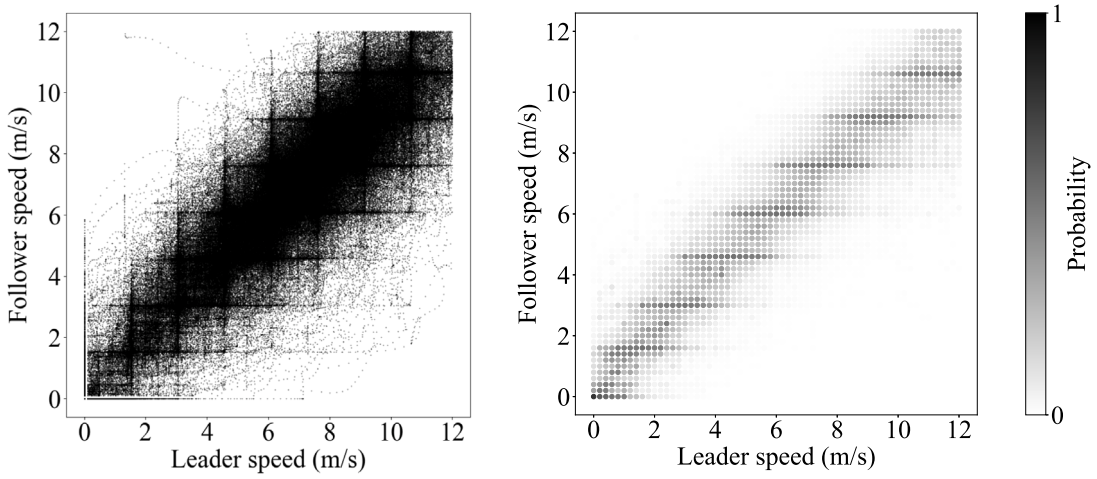

(a) Scatter of follower speed vs. leader speed (b) Empirical speed conditional distribution

Fig. 4. Empirical speed conditional distribution extracted from NGSIM I-80 dataset.

Table 1
Hyperparameters and results of trained MDN for $P(S_i \mid V_i, V_{i-1})$ using NGSIM I-80 dataset.

Num of components M	Num of neurons in hidden layer	MAE (m)	MAPE
100	128	0.62	2.8%
Training data size	Training epoch		
160 072	15 000		

4.1.3. Stochastic fundamental diagram estimation

In this section, we apply the proposed framework to derive the SFD from the microscopic model. We first substitute the complete microscopic model, which is the product of the empirical speed conditional distribution $P(V_i = v_e \mid V_{i-1} = v_e)$ and trained MDN for $P(S_i \mid V_i = v_e, V_{i-1} = v_e)$, into Eq. (8) to obtain the joint distribution for the platoon under equilibrium. Under the special case of HV-HV pairs only in the platoon, the joint distribution of speed and density $P\left(V = v_e, K\right)$ is then obtained using Eqs. (9)–(11), and the SFD modeled as $P\left(Q \mid K\right)$ is further derived with Eq. (12) utilizing the speed-density-flow relationship. Numerically, we enumerate equilibrium speeds v_e and corresponding equilibrium spacings, and then calculate the resulting flow-density points with their probabilities.

The estimated SFD is presented in Fig. 5(a), where a deeper green represents a higher probability of flow for each density. Note that although the light green points appear uniform, they are varying low-probability states (most below 0.05), which is difficult to distinguish for the limited sensitivity of the color scale. Also due to the enumeration of equilibrium states, the estimated SFD is composed of multiple straight lines, where each one corresponds to a specific equilibrium speed. We compare the estimated SFD with empirical data, as shown in Fig. 5(b). To quantify the model's ability to capture variability in the FD, we use the Prediction Interval Coverage Probability (PICP) indicator (Jabari et al., 2014; Lei et al., 2024), which measures the proportion of empirical observations that lie within the predicted intervals. The high PICP value of 90.6% reinforces that most empirical data fall into the theoretically possible range in the flow-density space. Moreover, the estimated flow expectation closely aligns with the empirical results, with a MAPE of 9.1%, further validating the proposed framework.

4.2. Validation using simulation

4.2.1. Simulation setup

To further validate the proposed framework for its ability to accommodate heterogeneous leader–follower pairs, we conduct numerical simulation experiments using different Intelligent Driver Models (IDM) for four combinations. The IDM model, as a widely used CF model for both HV CF and AV CF behaviors (Punzo et al., 2021), is formulated as Treiber et al. (2000):

$$a_n(t) = a\left[1 - \left(\frac{v_n(t)}{v_0}\right)^4 - \left(\frac{s^*(t)}{s_n(t)}\right)^2\right] \tag{13a}$$

$$s^*(t) = s_0 + v_n(t)T + \frac{v_n(t)\left[v_n(t) - v_{n-1}(t)\right]}{2\sqrt{ab}} \tag{13b}$$

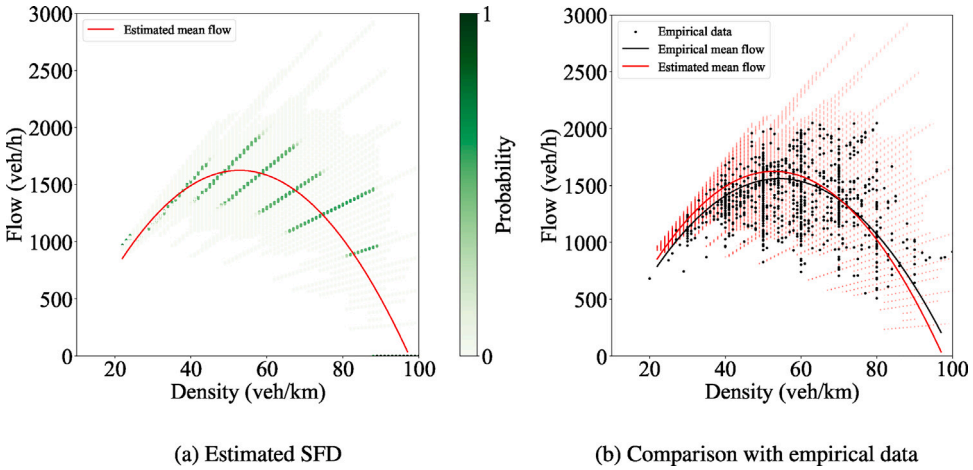

Fig. 5. Empirical and estimated SFD of NGSIM I-80 dataset.

Table 2
Calibrated parameters of IDM and results of trained MDN for 4 leader–follower pairs.

	IDM parameters						MDN results	
	T (s)	s_0 (m)	a (m/s^{-2})	b (m/s^{-2})	v_0 (m/s)	Δ%	MAE (m)	MAPE
HV-AV	1.13	2.24	1.58	1.19	18.7	50%	0.18	1.1%
HV-HV	1.17	3.28	1.84	1.29	19.1	20%	0.16	1.0%
AV-HV	1.55	5.22	1.87	1.02	18.6	5%	0.81	4.7%
AV-AV	0.82	5.83	0.34	4.92	28.7	1%	0.73	3.5%

where a is the maximum acceleration, v_0 is the desired speed, s_0 is the minimum gap, T is the desired time gap, b is the comfortable deceleration, $s^*(t)$ is the desired gap, $a_n(t), v_n(t), s_n(t)$ are the follower's acceleration, speed, spacing respectively, and $v_{n-1}(t)$ is the leader's speed.

We adopt calibrated IDM parameters for HV-AV, HV-HV and AV-HV pairs using the Waymo dataset (Hu et al., 2023). Due to the sparsity of AV trajectory datasets, the calibrated IDM may not be able to precisely replicate the CF behavior, but it is sufficiently accurate for validation purposes. Additionally, since the Waymo dataset does not include any AV-AV pairs, we calibrate the IDM for the AV-AV pair using the CF data of Adaptive Cruise Control (ACC) following ACC in the OpenACC dataset (Makridis et al., 2021). To further account for the stochastic CF behavior, we introduce a relative change in parameters, denoted as Δ%, according to the stochasticity level of leader–follower pairs in the empirical analysis (Jiao et al., 2024). All the parameters for 4 combinations are summarized in Table 2.

Using these CF models for different leader–follower pairs, we perform numerical simulations on a 300 m single-lane ring road with a total of 20 vehicles (Sugiyama et al., 2008; Vinitsky et al., 2018) under various AV penetration rates. For each 600 s simulation run, the platoon arrangement is determined randomly, and each vehicle adopts the corresponding IDM model with parameters varying within the relative change for its leader–follower type. After 500 experiments for each AV penetration rate, we collect the simulated CF data to train the proposed microscopic model and aggregate the FD using a 100 m spatial interval and a 60 s time interval for validation.

4.2.2. Microscopic behavior learning

Based on the two-step microscopic model of leader–follower interactions, we first use the simulated CF data for each pair type to obtain the empirical conditional speed distribution $P(V_i \mid V_{i-1})$ by discretizing speeds, and then train the MDN for $P(S_i \mid V_i, V_{i-1})$ with the hyperparameters selected via grid search. As shown in Table 2, all the trained MDN achieves low MAE and MAPE within 0.9 m and 5% respectively, verifying its ability to learn the microscopic behavior from the data.

4.2.3. Stochastic fundamental diagram estimation

Following the proposed micro-macroscopic framework, we estimate the SFD based on the trained microscopic model under various AV penetration rates. For the sake of brevity, we only present the results under 15% AV in Fig. 6(a), where a darker green indicates a higher probability of flow for each density. To evaluate the accuracy of the estimated SFD, we compute the MAPE between estimated mean flow and simulation mean flow and the PICP of the stochastic estimation, which are 1.7% and 87.6% respectively. These results corroborate the visual observations in Fig. 6(b), demonstrating that the estimation is highly consistent with the simulation result and thus validating the effectiveness of the proposed framework.

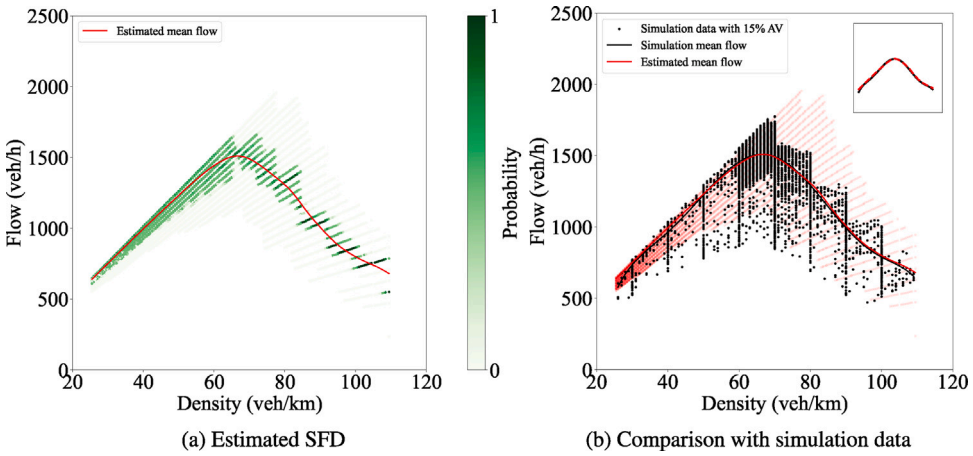

Fig. 6. Simulation and estimated SFD under 15% AV.

5. Case study in Waymo dataset

In this section, we apply the proposed framework to the Waymo Open Dataset to assess the impact of real-world AVs on traffic flow. Specifically, we learn the stochastic and heterogeneous leader–follower interactions from the Waymo dataset, based on which we derive the SFD of mixed traffic flow under varying AV penetration rates. This flexible framework further allows us to investigate mixed traffic management strategies, such as the design of AV spatial distribution and dedicated lanes, to enhance the performance.

5.1. Data preparation

The Waymo Open Dataset (Sun et al., 2020) offers a large scale of sensor data collected by AVs across various U.S. cities (i.e., San Francisco, Phoenix, and Mountain View). This dataset comprises 1000 segments, most from urban streets, each 20 s long, recorded at a high resolution of 0.1 s with a sophisticated sensor suite consisting of 5 LiDARs (1 mid-range and 4 short-range) and 5 cameras (front and sides). Utilizing these real-time sensor outputs with pre-built maps, the AV can thus pinpoint the positions of surrounding objects and itself.

To prepare this rich dataset for driving behavior modeling, a comprehensive process of restructuring, assessment, and enhancement is undertaken as per Hu et al. (2022). Particularly, the original data is transformed into a user-friendly tabular format, incorporating 25 essential attributes such as environment information, object features and object tracking trajectories. This processed dataset then undergoes rigorous quality assessments, including internal consistency analysis to ensure that position differentiation yield consistent velocity and acceleration, jerk analysis to identify anomalies. To further refine the data, an optimization-based outlier removal method is applied to eliminate extreme jerk and acceleration, followed by a wavelet denoising technique to filter out noise.

The resulting dataset yields 274 HV-AV pairs (53,737 data points), 1032 HV-HV pairs (200,125 data points), and 196 AV-HV pairs (38,493 data points). However, no AV-AV pairs exist in the current AV trajectory datasets as each segment contains at most one AV. Thus, we assume that the CF behavior of the AV-AV pair is equivalent to that of the AV-HV pair, which is reasonable for current AVs without connectivity and platooning capabilities. Notably, this assumption is made solely for this case study and does not compromise the generality of the proposed framework.

5.2. Microscopic behavior learning

Following the proposed formulation in Eq. (1), we learn the two-step leader–follower interaction for each type of pair. The first step of the speed conditional distribution $P(V_i \mid V_{i-1})$, is directly extracted from data by discretizing speeds with a step of 0.5 m/s. The second step is to determine the spacing given the leader and follower's speeds $P(S_i \mid V_i, V_{i-1})$, which is learned using the MDN. The optimal hyperparameters of the MDN for each type of pair are identified through grid search. In particular, we carefully tune hyperparameters, including the number of Gaussian components, the number of neurons in the hidden layer and training epochs, by systematically measuring performance across configurations. With the selected hyperparameters, we train the MDN for each type of pair, which is then evaluated using the MAE and the MAPE between estimated and empirical conditional expectations of spacing. All the parameters and results of the trained MDNs for HV-AV, HV-HV and AV-HV pairs are summarized in Table 3. From this table, we can see that all the MAE are below 1.7 m and all the MAPE are below 6%, showing a decent performance in modeling $P(S_i \mid V_i, V_{i-1})$ for all types of pairs.

Table 3
Hyperparameters and results of trained MDNs using Waymo dataset.

Leader–follower pair			MAE	MAPE
HV-AV	Num of components M 10	Num of neurons in hidden layer 64	1.69 m	6.0%
	Training data size 43 454	Training epoch 20 000		
HV-HV	Num of components M 100	Num of neurons in hidden layer 128	1.50 m	4.9%
	Training data size 153 721	Training epoch 15 000		
AV-HV	Num of components M 10	Num of neurons in hidden layer 64	1.69 m	5.3%
	Training data size 29 136	Training epoch 20 000		

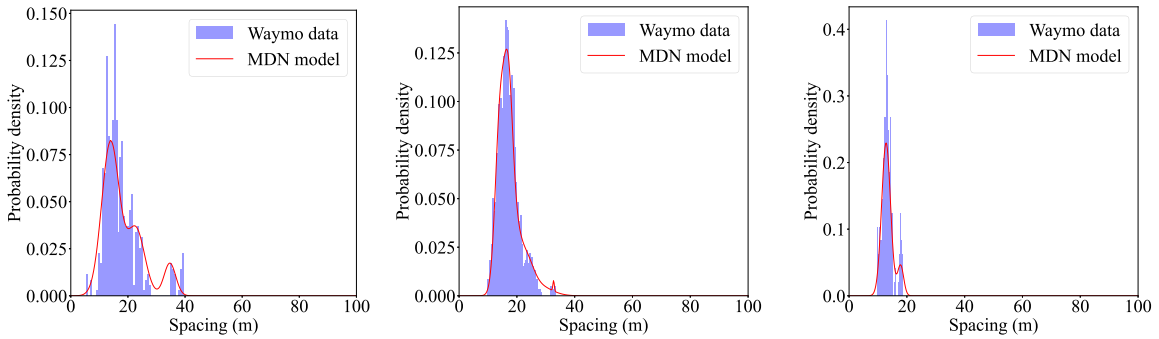

(a) HV-AV ($V_i = 7$m/s, $V_{i-1} = 6$m/s) (b) HV-HV ($V_i = 5$m/s, $V_{i-1} = 7$m/s) (c) AV-HV ($V_i = 1$m/s, $V_{i-1} = 2$m/s)

Fig. 7. Examples of MDN output distributions for each type of pair with Waymo dataset.

To intuitively illustrate the results of trained MDNs, we present the output distribution under given conditions for each type of leader–follower pair. As shown in Fig. 7, all the trained MDNs provide good approximations of the underlying multi-modal distributions, further validating the effectiveness of the MDN and the resulting microscopic model.

We further derive the equilibrium velocity-spacing relationship, also referred to as the microscopic fundamental diagram, to delineate the learned CF behavior. Specifically, we take identical equilibrium speed v_e for both the leader and follower, and then enumerate all possible equilibrium spacings to get their corresponding probabilities, i.e., $P(S_i = s_i \mid V_i = v_e, V_{i-1} = v_e)$, where $\sum_{s_i} P(S_i = s_i \mid V_i = v_e, V_{i-1} = v_e) = 1$. We present the microscopic fundamental diagram for each type of CF pair in Fig. 8, where a deeper green denotes a larger probability. For each equilibrium speed, the AV-HV pair generally has the largest equilibrium spacing with respect to other pairs, confirming the conservative behavior of AV. We also compare the variation of equilibrium spacing under each equilibrium speed, which reflects the uncertainty of CF behavior. Notably, HV-AV pairs show a larger variation of equilibrium spacing than HV-HV pairs, potentially caused by the curiosity of human drivers when following the AV. In contrast, AV-HV pairs exhibit a narrower range of equilibrium spacing (as indicated by the concentration of deeper green points) compared to HV-HV pairs, which is consistent with the stability of AV reported in earlier studies.

5.3. Stochastic fundamental diagram estimation

With the microscopic model learned from the Waymo dataset, in this subsection we utilize the proposed framework to derive the SFD of mixed traffic flow under different AV penetration rates. To be specific, we obtain the complete microscopic model $P(S_i, V_i \mid V_{i-1})$ for each type of leader–follower pair by combining the empirical conditional speed distribution $P(V_i \mid V_{i-1})$ and the trained MDN for $P(S_i \mid V_i, V_{i-1})$. The mixed platoon consisting of a composition of these pairs, characterized by the platoon configuration $\boldsymbol{C}$, is then modeled as the joint distribution $P(V, \boldsymbol{S} \mid \boldsymbol{C})$ using Eq. (9). Taking all the possible configurations of platoon arrangements into consideration under each AV penetration rate, assuming a random spatial distribution of AVs, the speed-density joint distribution $P(V, K)$ and the SFD, represented as $P(Q \mid K)$, are further derived under equilibrium using Eqs. (10)–(12).

We present the SFD results under relatively low penetration rates of the current Waymo AV (below 25%), as higher AV penetration rates may imply more advanced technologies that exhibit different CF behavior (e.g., smaller headway) compared to current AVs. As shown in Fig. 9, the green area represents the possible range in the flow-density space, with deeper green indicating higher probabilities (larger $P(Q \mid K = k)$ along the density k, where $\sum_q P(Q = q \mid K = k) = 1$), and the red curve denotes the mean flow-density relation. Clearly, the main feature of the flow-density relation, i.e., the well-known quadratic curve, is reproduced in

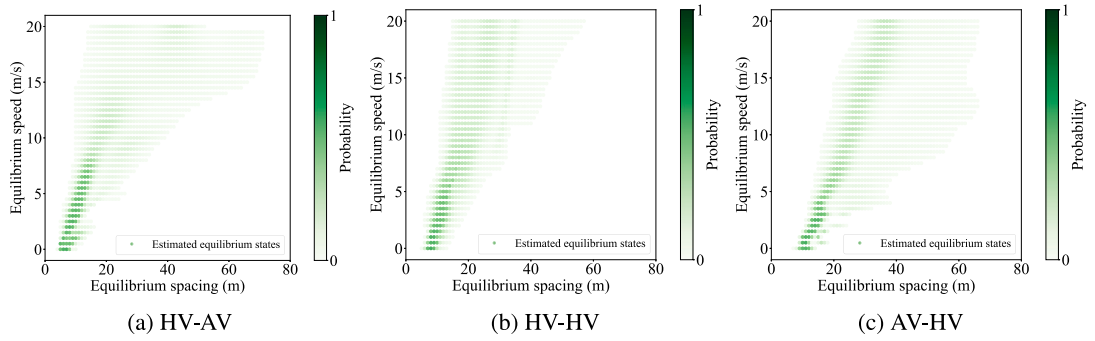

Fig. 8. Microscopic fundamental diagram for each type of pair in Waymo dataset.

all the estimated results. Note that due to the numerical enumeration of equilibrium speeds for the platoon, the resulting SFD is composed of multiple straight lines, each corresponding to a specific equilibrium speed.

To quantify the impact of AV penetration rates on mixed traffic flow, we further obtain the estimated mean capacity ($\mathbb{E}[Q_c]$), the standard deviation of capacity ($\sigma[Q_c]$), critical density (k_c) and conditional entropy ($\mathbb{H}(Q \mid K)$) for various AV penetration rates. The estimated mean capacity and critical density measure the efficiency of the mixed traffic flow, while the standard deviation of capacity and conditional entropy represent the stochasticity of the estimated capacity and the whole flow-density relation.

As shown in the left column of Fig. 10, the mean capacity decreases with more AVs while remaining relatively stable under 15%–25% AV penetration. Similarly, the critical density drops with higher AV penetration rates. On the other hand, in the right column of Fig. 10, we can see that the standard deviation of capacity declines within 10% AV before a slight increase, while the conditional entropy gently rises with the AV penetration rate. Taken together, the mixed traffic flow with a higher proportion of AVs becomes less efficient for the conservative AV behavior, exhibiting lower mean capacity and critical density. While its uncertainty in capacity decreases due to more predictable actions of AVs. However, as the AV penetration rate increases and more platoon arrangements form, the uncertainty starts to rise subtly, which is also reflected in the modestly growing entropy of the flow-density relation that represents the overall stochasticity.

These results accord with earlier empirical investigations on real-world AVs (Hu et al., 2023; Alhariqi et al., 2023; Jiang et al., 2024b; Ren et al., 2024; Zhong et al., 2024), consistently reflecting that the present AV is more stable yet conservative and thus potentially results in negative effects on traffic flow. However, previous simulation-based studies, which use unrealistic and over-simplified assumptions about the headway or specific CF models, always suggest that increasing AV penetration leads to more efficient traffic flow (Talebpour and Mahmassani, 2016; Guan et al., 2023; Jiang et al., 2024b). This discrepancy further highlights the necessity of employing real-world AV datasets in mixed traffic modeling.

5.4. Evaluation of mixed traffic management strategies

Given the reduced efficiency of mixed traffic with higher AV penetration, a natural question arises: how can we enhance the performance? To answer this question, we utilize the proposed framework to analyze the impacts of commonly used management strategies, i.e., AV spatial distributions and dedicated lanes, on the SFD of mixed traffic, see Fig. 11. Our findings, together with the proposed framework, provide transportation planners and policymakers with actionable strategies to optimize mixed traffic and practical tools to rigorously evaluate their effectiveness.

5.4.1. Impacts of AV spatial distribution

Platooning of AVs is widely recognized for its potential to enhance traffic efficiency, driving safety, and lower fuel consumption (Li et al., 2022a; Shladover et al., 2015). Even without connectivity capability, this prevailing AV platoon formation may suppress the stochasticity of traffic flow by grouping AV and HV respectively, thereby improving the overall system performance. We thus evaluate the SFD of the mixed traffic under AV platooning, with the random distribution of AV serving as the baseline.

We present the relative change in mean capacity and standard deviation of capacity in Fig. 12, prioritizing these key metrics while omitting others for brevity. From the figure, it can be seen that the mean capacity remains almost the same, showing a slight increase of up to 1.5% within 20% AV penetration, while it falls to negative values beyond it compared to the random AV distribution. A possible explanation for this fall might be that randomly distributed AVs are more likely to produce a larger number of HV-AV pairs than AV platooning with higher AV penetration rates, where the HV-AV pair is reported to maintain a shorter distance and time headway than other type of pairs. The standard deviation of capacity mainly decreases as expected and achieves a maximum of 26.7% drop with 15% AV. In summary, AV platooning with current AV capabilities modestly improves the efficiency while largely reducing the uncertainty at 15% AV penetration.

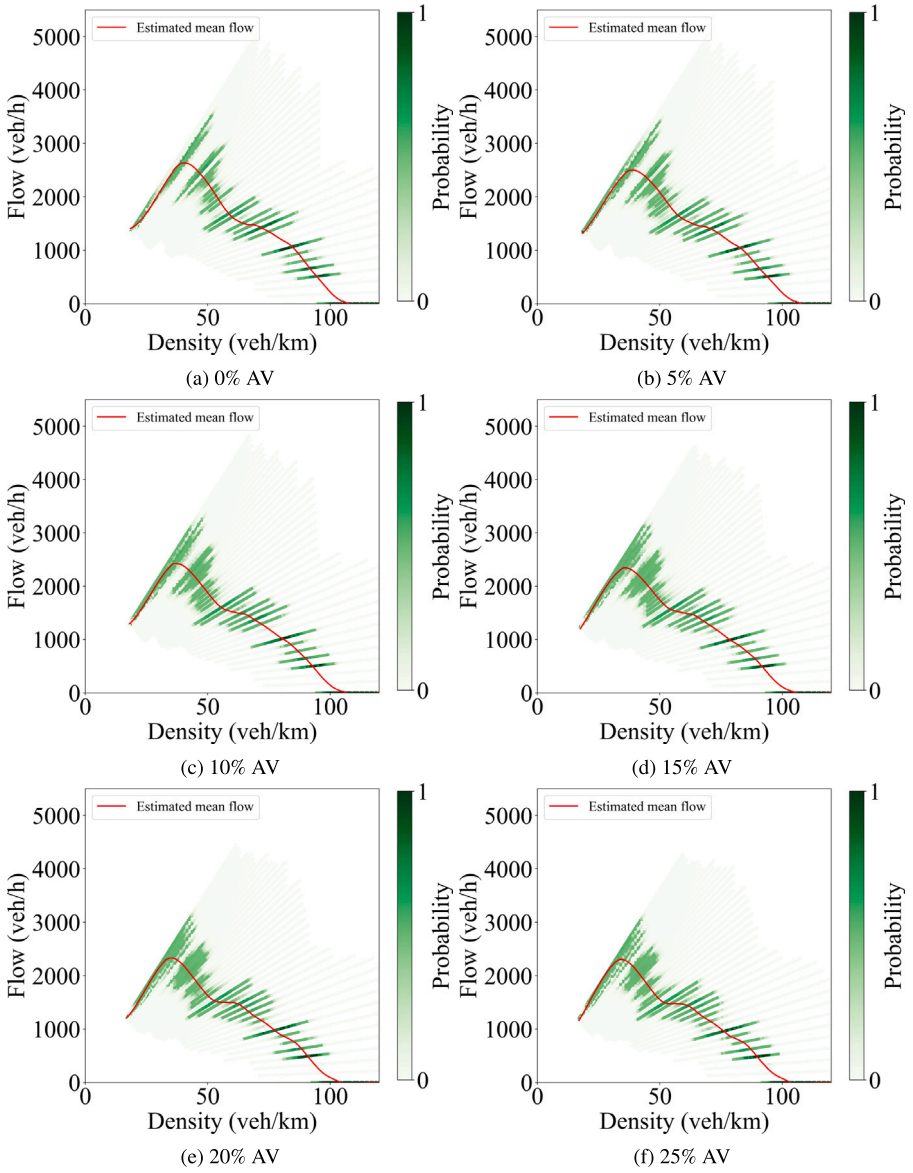

Fig. 9. Estimated SFD results using Waymo dataset under different AV penetration rates.

5.4.2. Impacts of lane management

Current AVs tend to perturb the traffic flow due to their conservative behaviors. To mitigate these perturbations and improve traffic performance, exclusive lanes emerge as a promising management strategy. We thus assess the impacts of AV-exclusive lanes and HV-exclusive lanes on the SFD in terms of the relative changes in mean capacity and its standard deviation. In both experiments, we compare hybrid lane configurations involving exclusive lanes against a baseline of mixed-traffic lanes within 25% AV penetration, where all mixed-traffic lanes assume randomly distributed AVs.

For the AV-exclusive lane strategy, we examine the case of 1 AV-exclusive lane and 3 mixed-traffic lanes against 4 lanes of mixed traffic. Mathematically, given the AV penetration rate p in 4 mixed-traffic lanes and the corresponding capacity $Q_c(p)$, the AV penetration rate in the 3 mixed-traffic lanes with other 1 AV-exclusive lane is derived as:

$$p' = \frac{lpQ_c(p) - l_aQ_c(p=1)}{lQ_c(p) - l_aQ_c(p=1)} \tag{14}$$

where $l = 4$, $l_a = 1$ are the number of total lanes and AV-exclusive lanes. The capacity of 1 AV-exclusive lanes and 3 mixed-traffic lanes is then given as:

$$Q_c' = \frac{l_a}{l}\min\left(lpQ_c(p), Q_c(p=1)\right) + (1 - \frac{l_a}{l})Q_c(p') \tag{15}$$

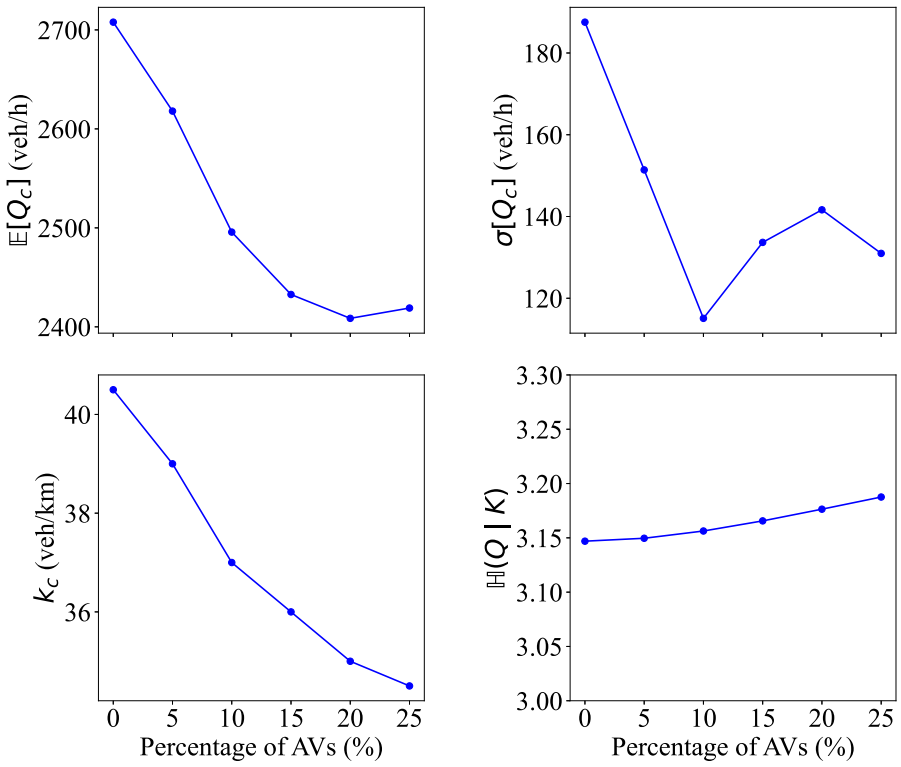

Fig. 10. Evaluation metrics of the mixed traffic flow under different AV penetration rates.

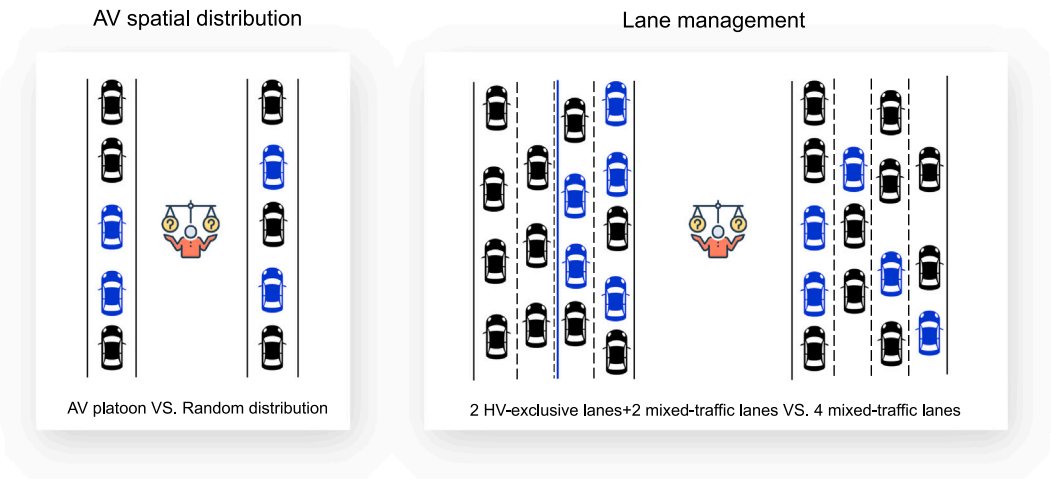

Fig. 11. Assessing mixed traffic management strategies: an analysis of two cases.

Fig. 13 presents the corresponding SFD results. The mean capacity generally decreases within 15% AV penetration, and the standard deviation of capacity begins to noticeably drop beyond 20%. At 20% AV penetration, implementing an AV-exclusive lane yields a 4.3% improvement in mean capacity, while the standard deviation remains nearly unchanged.

For the HV-exclusive lane strategy, we compare the SFD results of 2 HV-exclusive lanes and 2 mixed-traffic lanes against 4 lanes of mixed traffic within 25% AV penetration as a demonstration. Note that for this strategy to be effective, sufficient mixed-lane must be allocated to accommodate the expected AV flow.

Similarly, the AV penetration rate in the 2 mixed-traffic lanes with other 2 HV-exclusive lanes is:

$$p'' = \frac{l p Q_c(p)}{l Q_c(p) - l_h Q_c(p=0)} \tag{16}$$

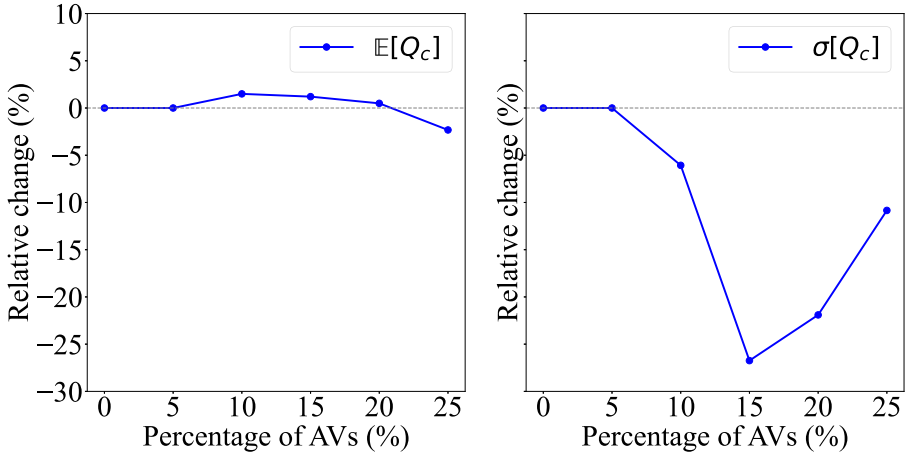

Fig. 12. SFD results of AV platooning compared to random distribution.

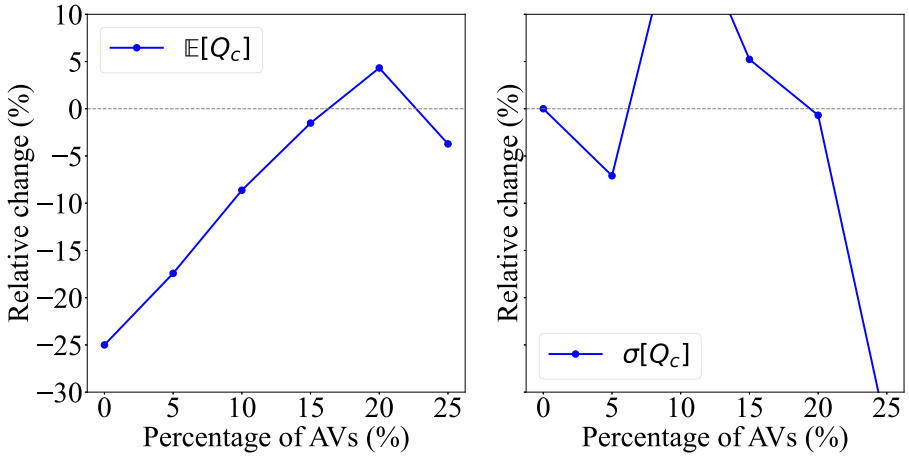

Fig. 13. SFD results of 1 AV-exclusive lane + 3 mixed-traffic lanes compared to 4 mixed-traffic lanes.

where $l = 4$, $l_h = 2$ are the number of total lanes and HV-exclusive lanes. We then derive the capacity of 2 HV-exclusive lanes and 2 mixed-traffic lanes:

$$Q_c'' = \frac{l_h}{l} Q_c(p = 0) + (1 - \frac{l_h}{l}) Q_c(p'') \tag{17}$$

As shown in Fig. 14, this strategy leads to consistent capacity gains and remarkable reductions in uncertainty. At 20% AV penetration, the implementation of HV-exclusive lanes enables a 4.5% increase in mean capacity and a 21.3% reduction in its standard deviation, highlighting the effectiveness of HV-exclusive lane management strategy.

Overall, the proposed framework offers a practical tool to devise and evaluate mixed traffic management strategies. The examples of AV platooning and exclusive lanes demonstrate that these strategies can mitigate stochasticity and enhance efficiency at certain AV penetration rates. Among these strategies, HV-exclusive lanes show greater effectiveness with larger improvements. However, it is noteworthy that even with these traffic management strategies in place, the mean capacity of mixed traffic flow does not exceed that of pure HV traffic flow. This underscores the need for cooperative control through connected AVs to further optimize the mixed traffic system.

6. Conclusion

This study presents a novel data-driven framework to model the SFD of mixed traffic flow. Specifically, we first learn the microscopic interaction, modeled as a two-step conditional distribution, from AV datasets using the MDN for various leader–follower pairs. The mixed platoon, composed of these pairs, is characterized by a joint distribution with Markov chain modeling. By incorporating platoon arrangements with the law of total probability, we derive the SFD of mixed traffic flow. The proposed framework accurately reproduces the empirical FD with the NGSIM I-80 dataset, demonstrating its efficacy.

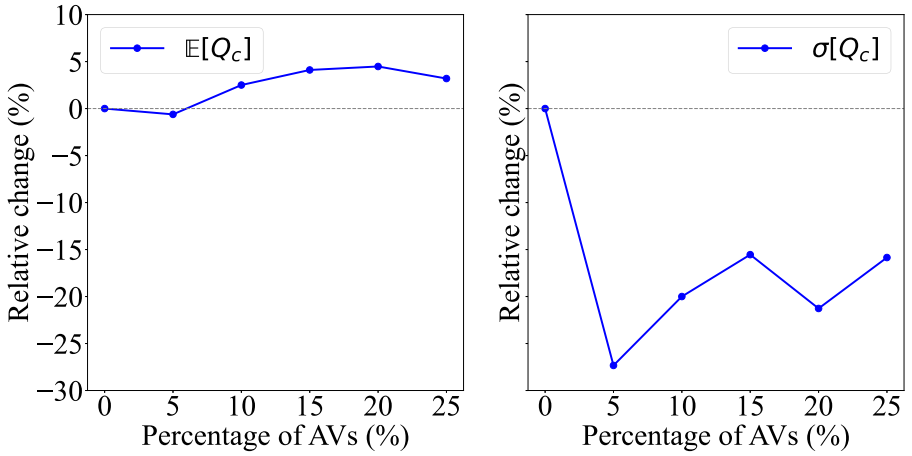

Fig. 14. SFD results of 2 HV-exclusive lanes + 2 mixed-traffic lanes compared to 4 mixed-traffic lanes.

We apply the proposed framework to the Waymo dataset as a case study, and the results reveal that as AV penetration rates increase, the uncertainty of the mixed traffic generally decreases, as evidenced by a lower standard deviation of capacity, which leads to improved reliability and smoother operation. However, this comes at the cost of reduced traffic efficiency, as indicated by declines in mean capacity and critical density. These findings corroborate the stable yet conservative AV behaviors observed in previous empirical studies, further verifying the effectiveness of the proposed framework.

In summary, this framework provides a general guideline to derive the SFD of mixed traffic from empirical data, capturing the stochasticity in heterogeneous CF behaviors and diverse platoon arrangements. By accounting for these uncertainties, this work enables a more comprehensive understanding of real-world AVs for their traffic-level impacts. To mitigate the negative impacts, appropriate mixed traffic management strategies, such as the AV platooning and HV-exclusive lanes as demonstrated in this study, can be further applied and assessed by the proposed framework. Looking ahead, future research could integrate connected AV capabilities and explore advanced traffic management strategies.

CRediT authorship contribution statement

Xiaohui Zhang: Writing – original draft, Validation, Software, Methodology, Conceptualization. **Kaidi Yang:** Writing – review & editing, Validation, Methodology, Funding acquisition, Conceptualization. **Jie Sun:** Writing – review & editing, Validation. **Jian Sun:** Writing – review & editing, Validation, Funding acquisition, Conceptualization.

Declaration of competing interest

The authors declare that they have no known competing financial interests or personal relationships that could have appeared to influence the work reported in this paper.

Acknowledgments

The authors would like to acknowledge the support provided by the program of the China Scholarship Council (No. 202306260117), the Singapore Ministry of Education (MOE) under its Academic Research Fund Tier 1 (A-8001183-00-00), and the National Natural Science Foundation of China (52125208).

Appendix. Notations

Name	Notation	Name	Notation
Random variables		**Variables**	
Speed of vehicle i	V_i	Total number of vehicles in the platoon	n
Spacing between vehicle i and its leader	S_i	AV penetration rate	p
Configuration of the platoon arrangement	$\boldsymbol{C}$	Number of HV-AV pairs in the platoon	n_{HA}
Equilibrium speed	V	Number of HV-HV pairs in the platoon	n_{HH}
Equilibrium density	K	Number of AV-HV pairs in the platoon	n_{AH}
Equilibrium flow	Q	Number of AV-AV pairs in the platoon	n_{AA}
Equilibrium capacity	Q_c	Critical density	k_c

Data availability

The code used in this study is openly available at: https://github.com/tjzxh/SFD-modeling-of-mixed-traffic.git.

References

Alhariqi, A., Gu, Z., Saberi, M., 2023. Impact of vehicle arrangement in mixed autonomy traffic on emissions. Transp. Res. Part D: Transp. Environ. 125, 103964. http://dx.doi.org/10.1016/j.trd.2023.103964, URL: https://linkinghub.elsevier.com/retrieve/pii/S1361920923003619.

Bishop, C.M., 1994. Mixture Density Networks. Technical Report, Aston University, Birmingham, URL: https://research.aston.ac.uk/en/publications/mixture-density-networks.

Bishop, C.M., 2006. Pattern Recognition and Machine Learning. Springer New York, http://dx.doi.org/10.1007/978-0-387-45528-0, URL: https://link.springer.com/deleted.

Brackstone, M., McDonald, M., 1999. Car-following: a historical review. Transp. Res. Part F: Traffic Psychol. Behav. 2 (4), 181–196. http://dx.doi.org/10.1016/S1369-8478(00)00005-X, URL: https://linkinghub.elsevier.com/retrieve/pii/S136984780000005X.

Branston, D., 1976. Models of single lane time headway distributions. Transp. Sci. 10 (2), 125–148. http://dx.doi.org/10.1287/trsc.10.2.125, URL: https://pubsonline.informs.org/doi/10.1287/trsc.10.2.125.

Caesar, H., Bankiti, V., Lang, A.H., Vora, S., Liong, V.E., Xu, Q., Krishnan, A., Pan, Y., Baldan, G., Beijbom, O., 2020. Nuscenes: A multimodal dataset for autonomous driving. In: 2020 IEEE/CVF Conference on Computer Vision and Pattern Recognition. CVPR, IEEE, pp. 11618–11628. http://dx.doi.org/10.1109/CVPR42600.2020.01164, URL: https://ieeexplore.ieee.org/document/9156412/.

Caruana, R., 1997. Multitask learning. Mach. Learn. 28 (1), 41–75. http://dx.doi.org/10.1023/A:1007379606734, URL: https://link.springer.com/article/10.1023/A:1007379606734.

Choi, S., Lee, K., Lim, S., Oh, S., 2018. Uncertainty-aware learning from demonstration using mixture density networks with sampling-free variance modeling. In: 2018 IEEE International Conference on Robotics and Automation. ICRA, IEEE, pp. 6915–6922. http://dx.doi.org/10.1109/ICRA.2018.8462978, URL: https://ieeexplore.ieee.org/document/8462978/.

Coifman, B., 2015. Empirical flow-density and speed-spacing relationships: Evidence of vehicle length dependency. Transp. Res. Part B: Methodol. 78, 54–65. http://dx.doi.org/10.1016/j.trb.2015.04.006, URL: https://linkinghub.elsevier.com/retrieve/pii/S0191261515000818.

Daganzo, C.F., 2002. A behavioral theory of multi-lane traffic flow. Part I: Long homogeneous freeway sections. Transp. Res. Part B: Methodol. 36 (2), 131–158. http://dx.doi.org/10.1016/S0191-2615(00)00042-4, URL: https://linkinghub.elsevier.com/retrieve/pii/S0191261500000424.

Edie, L., 1963. Discussion of traffic stream measurements and definitions. In: 2nd International Symposium on the Theory of Traffic Flow.

Guan, H., Wang, H., Meng, Q., Mak, C.L., 2023. Markov chain-based traffic analysis on platooning effect among mixed semi- and fully-autonomous vehicles in a freeway lane. Transp. Res. Part B: Methodol. 173, 176–202. http://dx.doi.org/10.1016/j.trb.2023.04.006, URL: https://linkinghub.elsevier.com/retrieve/pii/S0191261523000693.

Hoogendoorn, S.P., Bovy, P.H.L., 1998. New estimation technique for vehicle-type-specific headway distributions. Transp. Res. Rec.: J. Transp. Res. Board 1646 (1), 18–28. http://dx.doi.org/10.3141/1646-03, URL: http://journals.sagepub.com/doi/10.3141/1646-03.

Houston, J., Zuidhof, G., Bergamini, L., Ye, Y., Chen, L., Jain, A., Omari, S., Iglovikov, V., Ondruska, P., 2021. One thousand and one hours: Self-driving motion prediction dataset. In: Kober, J., Ramos, F., Tomlin, C. (Eds.), Proceedings of the 2020 Conference on Robot Learning. In: Proceedings of Machine Learning Research, vol. 155, PMLR, pp. 409–418, URL: https://proceedings.mlr.press/v155/houston21a.html.

Hu, X., Zheng, Z., Chen, D., Sun, J., 2023. Autonomous vehicle's impact on traffic: Empirical evidence from waymo open dataset and implications from modelling. IEEE Trans. Intell. Transp. Syst. 24 (6), 6711–6724. http://dx.doi.org/10.1109/TITS.2023.3258145, URL: https://ieeexplore.ieee.org/document/10078438/.

Hu, X., Zheng, Z., Chen, D., Zhang, X., Sun, J., 2022. Processing, assessing, and enhancing the waymo autonomous vehicle open dataset for driving behavior research. Transp. Res. Part C: Emerg. Technol. 134, 103490. http://dx.doi.org/10.1016/j.trc.2021.103490, URL: https://linkinghub.elsevier.com/retrieve/pii/S0968090X21004769.

Jabari, S.E., Liu, H.X., 2012. A stochastic model of traffic flow: Theoretical foundations. Transp. Res. Part B: Methodol. 46 (1), 156–174. http://dx.doi.org/10.1016/j.trb.2011.09.006, URL: https://linkinghub.elsevier.com/retrieve/pii/S0191261511001354.

Jabari, S.E., Zheng, J., Liu, H.X., 2014. A probabilistic stationary speed–density relation based on Newell's simplified car-following model. Transp. Res. Part B: Methodol. 68, 205–223. http://dx.doi.org/10.1016/j.trb.2014.06.006, URL: https://linkinghub.elsevier.com/retrieve/pii/S0191261514001131.

Jiang, Y., Chen, H., Cong, H., Wu, Y., Yao, Z., 2024b. Fundamental diagram of mixed traffic flow of CAVs with different connectivity and automation levels. Phys. A 646, 129904. http://dx.doi.org/10.1016/j.physa.2024.129904, URL: https://linkinghub.elsevier.com/retrieve/pii/S0378437124004138.

Jiang, J., Zhou, Y., Wang, X., Ahn, S., 2024a. On dynamic fundamental diagrams: Implications for automated vehicles. Transp. Res. Part B: Methodol. 189, 102979. http://dx.doi.org/10.1016/j.trb.2024.102979, URL: https://linkinghub.elsevier.com/retrieve/pii/S0191261524001036.

Jiao, Y., Li, G., Calvert, S.C., van Cranenburgh, S., van Lint, H., 2024. Beyond behavioural change: Investigating alternative explanations for shorter time headways when human drivers follow automated vehicles. Transp. Res. Part C: Emerg. Technol. 164, 104673. http://dx.doi.org/10.1016/j.trc.2024.104673, URL: https://linkinghub.elsevier.com/retrieve/pii/S0968090X24001943.

Johnson, N.L., Kemp, A.W., Kotz, S., 2005. Univariate discrete distributions. Wiley Series in Probability and Statistics, Wiley, http://dx.doi.org/10.1002/0471715816, URL: https://onlinelibrary.wiley.com/doi/book/10.1002/0471715816.

Jospin, L.V., Laga, H., Boussaid, F., Buntine, W., Bennamoun, M., 2022. Hands-on Bayesian neural networks—A tutorial for deep learning users. IEEE Comput. Intell. Mag. 17 (2), 29–48. http://dx.doi.org/10.1109/MCI.2022.3155327, URL: https://ieeexplore.ieee.org/document/9756596/.

Kerner, B.S., 2009. Introduction to modern traffic flow theory and control. Introduction To Modern Traffic Flow Theory and Control: The Long Road To Three-Phase Traffic Theory. Springer Berlin Heidelberg, Berlin, Heidelberg, pp. 1–265. http://dx.doi.org/10.1007/978-3-642-02605-8, URL: https://link.springer.com/10.1007/978-3-642-02605-8.

Keyvan-Ekbatani, M., Kouvelas, A., Papamichail, I., Papageorgiou, M., 2012. Exploiting the fundamental diagram of urban networks for feedback-based gating. Transp. Res. Part B: Methodol. 46 (10), 1393–1403. http://dx.doi.org/10.1016/j.trb.2012.06.008, URL: https://linkinghub.elsevier.com/retrieve/pii/S0191261512000926.

Kingma, D.P., Ba, J., 2014. Adam: A method for stochastic optimization. In: 3rd International Conference on Learning Representations. In: ICLR 2015- Conference Track Proceedings, URL: http://arxiv.org/abs/1412.6980.

Lapardhaja, S., Doig Godier, J., Cassidy, M.J., (David) Kan, X., 2024. ACC, queue storage, and worrisome news for cities. Transp. Res. Part C: Emerg. Technol. 167, 104809. http://dx.doi.org/10.1016/J.TRC.2024.104809.

Lei, Y., Gong, Y., Yang, X.T., 2024. Unraveling stochastic fundamental diagrams with empirical knowledge: modeling, limitations, and future directions. Transp. Res. Part C: Emerg. Technol. 169, 104851. http://dx.doi.org/10.1016/j.trc.2024.104851, URL: https://linkinghub.elsevier.com/retrieve/pii/S0968090X24003723.

Li, T., Chen, D., Zhou, H., Xie, Y., Laval, J., 2022b. Fundamental diagrams of commercial adaptive cruise control: Worldwide experimental evidence. Transp. Res. Part C: Emerg. Technol. 134, 103458. http://dx.doi.org/10.1016/j.trc.2021.103458, URL: https://linkinghub.elsevier.com/retrieve/pii/S0968090X21004460.

Li, C., Lee, G.H., 2019. Generating multiple hypotheses for 3D human pose estimation with mixture density network. In: 2019 IEEE/CVF Conference on Computer Vision and Pattern Recognition. CVPR, vol. 2019-June, IEEE, pp. 9879–9887. http://dx.doi.org/10.1109/CVPR.2019.01012, URL: https://ieeexplore.ieee.org/document/8953904/.

Li, K., Wang, J., Zheng, Y., 2022a. Cooperative formation of autonomous vehicles in mixed traffic flow: Beyond platooning. IEEE Trans. Intell. Transp. Syst. 23 (9), 15951–15966. http://dx.doi.org/10.1109/TITS.2022.3146612, URL: https://ieeexplore.ieee.org/document/9709187/.

Liu, Z., Lyu, C., Wang, Z., Wang, S., Liu, P., Meng, Q., 2023. A Gaussian-process-based data-driven traffic flow model and its application in road capacity analysis. IEEE Trans. Intell. Transp. Syst. 24 (2), 1–20. http://dx.doi.org/10.1109/TITS.2022.3223982, URL: https://ieeexplore.ieee.org/document/10025463/.

Liu, M., Yurtsever, E., Fossaert, J., Zhou, X., Zimmer, W., Cui, Y., Zagar, B.L., Knoll, A.C., 2024. A survey on autonomous driving datasets: Statistics, annotation quality, and a future outlook. ArXiv URL: http://arxiv.org/abs/2401.01454.

Mahnke, R., Kaupužs, J., 1999. Stochastic theory of freeway traffic. Phys. Rev. E 59 (1), 117–125. http://dx.doi.org/10.1103/PhysRevE.59.117, URL: https://link.aps.org/doi/10.1103/PhysRevE.59.117.

Makridis, M., Mattas, K., Anesiadou, A., Ciuffo, B., 2021. OpenACC. An open database of car-following experiments to study the properties of commercial ACC systems. Transp. Res. Part C: Emerg. Technol. 125, 103047. http://dx.doi.org/10.1016/j.trc.2021.103047, URL: https://linkinghub.elsevier.com/retrieve/pii/S0968090X21000772.

Martínez-Díaz, M., Al-Haddad, C., Soriguera, F., Antoniou, C., 2024. Impacts of platooning of connected automated vehicles on highways. IEEE Trans. Intell. Transp. Syst. 25 (7), 6366–6396. http://dx.doi.org/10.1109/TITS.2024.3350776, URL: https://ieeexplore.ieee.org/document/10417852/.

Montanino, M., Punzo, V., 2015. Trajectory data reconstruction and simulation-based validation against macroscopic traffic patterns. Transp. Res. Part B: Methodol. 80, 82–106. http://dx.doi.org/10.1016/j.trb.2015.06.010, URL: https://linkinghub.elsevier.com/retrieve/pii/S0191261515001393.

Montanino, M., Punzo, V., 2021. On string stability of a mixed and heterogeneous traffic flow: A unifying modelling framework. Transp. Res. Part B: Methodol. 144, 133–154. http://dx.doi.org/10.1016/j.trb.2020.11.009, URL: https://linkinghub.elsevier.com/retrieve/pii/S0191261520304409.

Punzo, V., Zheng, Z., Montanino, M., 2021. About calibration of car-following dynamics of automated and human-driven vehicles: Methodology, guidelines and codes. Transp. Res. Part C: Emerg. Technol. 128, 103165. http://dx.doi.org/10.1016/j.trc.2021.103165, URL: https://linkinghub.elsevier.com/retrieve/pii/S0968090X21001832.

Qu, X., Zhang, J., Wang, S., 2017. On the stochastic fundamental diagram for freeway traffic: Model development, analytical properties, validation, and extensive applications. Transp. Res. Part B: Methodol. 104, 256–271. http://dx.doi.org/10.1016/j.trb.2017.07.003, URL: https://linkinghub.elsevier.com/retrieve/pii/S0191261516306622.

Ren, X., Bai, L., Zheng, Y., Han, Y., Liu, P., 2024. Mixed traffic capacity estimation of autonomous vehicles impact based on empirical data. Appl. Math. Model. 135, 193–211. http://dx.doi.org/10.1016/j.apm.2024.06.041, URL: https://linkinghub.elsevier.com/retrieve/pii/S0307904X24003214.

Sedgewick, R., 1977. Permutation generation methods. ACM Comput. Surv. 9 (2), 137–164. http://dx.doi.org/10.1145/356689.356692, URL: https://dl.acm.org/doi/10.1145/356689.356692.

Shang, M., Stern, R.E., 2021. Impacts of commercially available adaptive cruise control vehicles on highway stability and throughput. Transp. Res. Part C: Emerg. Technol. 122, 102897. http://dx.doi.org/10.1016/j.trc.2020.102897, URL: https://linkinghub.elsevier.com/retrieve/pii/S0968090X2030797X.

Shi, X., Li, X., 2021. Constructing a fundamental diagram for traffic flow with automated vehicles: Methodology and demonstration. Transp. Res. Part B: Methodol. 150, 279–292. http://dx.doi.org/10.1016/j.trb.2021.06.011, URL: https://linkinghub.elsevier.com/retrieve/pii/S0191261521001235.

Shladover, S.E., Nowakowski, C., Lu, X.-Y., Ferlis, R., 2015. Cooperative adaptive cruise control. Transp. Res. Rec.: J. Transp. Res. Board 2489 (1), 145–152. http://dx.doi.org/10.3141/2489-17, URL: http://journals.sagepub.com/doi/10.3141/2489-17.

Sugiyama, Y., Fukui, M., Kikuchi, M., Hasebe, K., Nakayama, A., Nishinari, K., Tadaki, S.-i., Yukawa, S., 2008. Traffic jams without bottlenecks—experimental evidence for the physical mechanism of the formation of a jam. New J. Phys. 10 (3), 033001. http://dx.doi.org/10.1088/1367-2630/10/3/033001, URL: https://iopscience.iop.org/article/10.1088/1367-2630/10/3/033001.

Sun, P., Kretzschmar, H., Dotiwalla, X., Chouard, A., Patnaik, V., Tsui, P., Guo, J., Zhou, Y., Chai, Y., Caine, B., Vasudevan, V., Han, W., Ngiam, J., Zhao, H., Timofeev, A., Ettinger, S., Krivokon, M., Gao, A., Joshi, A., Zhang, Y., Shlens, J., Chen, Z., Anguelov, D., 2020. Scalability in perception for autonomous driving: Waymo open dataset. In: 2020 IEEE/CVF Conference on Computer Vision and Pattern Recognition. CVPR, IEEE, pp. 2443–2451. http://dx.doi.org/10.1109/CVPR42600.2020.00252, URL: https://ieeexplore.ieee.org/document/9156973/.

Talebpour, A., Mahmassani, H.S., 2016. Influence of connected and autonomous vehicles on traffic flow stability and throughput. Transp. Res. Part C: Emerg. Technol. 71, 143–163. http://dx.doi.org/10.1016/J.TRC.2016.07.007.

Treiber, M., Hennecke, A., Helbing, D., 2000. Congested traffic states in empirical observations and microscopic simulations. Phys. Rev. E 62 (2), 1805–1824. http://dx.doi.org/10.1103/PhysRevE.62.1805, URL: https://link.aps.org/doi/10.1103/PhysRevE.62.1805.

Treiber, M., Kesting, A., 2013. Traffic flow dynamics. Traffic Flow Dynamics: Data, Models and Simulation. Springer Berlin Heidelberg, Berlin, Heidelberg, pp. 1–503. http://dx.doi.org/10.1007/978-3-642-32460-4, URL: https://link.springer.com/10.1007/978-3-642-32460-4.

Treiber, M., Kesting, A., Helbing, D., 2006. Understanding widely scattered traffic flows, the capacity drop, and platoons as effects of variance-driven time gaps. Phys. Rev. E 74 (1), 016123. http://dx.doi.org/10.1103/PhysRevE.74.016123, URL: https://link.aps.org/doi/10.1103/PhysRevE.74.016123.

Vinitsky, E., Kreidieh, A., Flem, L.L., Kheterpal, N., Jang, K., Wu, C., Wu, F., Liaw, R., Liang, E., Bayen, A.M., 2018. Benchmarks for Reinforcement Learning in Mixed-Autonomy Traffic. PMLR, pp. 399–409, URL: https://proceedings.mlr.press/v87/vinitsky18a.html.

Wang, S., Chen, X., Qu, X., 2021. Model on empirically calibrating stochastic traffic flow fundamental diagram. Commun. Transp. Res. 1, 100015. http://dx.doi.org/10.1016/j.commtr.2021.100015, URL: https://linkinghub.elsevier.com/retrieve/pii/S2772424721000159.

Wang, Y., Farah, H., Yu, R., Qiu, S., van Arem, B., 2023. Characterizing behavioral differences of autonomous vehicles and human-driven vehicles at signalized intersections based on Waymo open dataset. Transp. Res. Rec.: J. Transp. Res. Board 2677 (11), 324–337. http://dx.doi.org/10.1177/03611981231165783, URL: http://journals.sagepub.com/doi/10.1177/03611981231165783.

Wang, Y., Xu, Z., Wu, Y., Jiang, Y., Yao, Z., 2025. Fundamental diagram modeling of mixed traffic flow considering dedicated lanes for human-driven vehicles. IEEE Trans. Veh. Technol. 1–16. http://dx.doi.org/10.1109/TVT.2025.3541387, URL: https://ieeexplore.ieee.org/document/10884053/.

Wen, X., Cui, Z., Jian, S., 2022. Characterizing car-following behaviors of human drivers when following automated vehicles using the real-world dataset. Accid. Anal. Prev. 172, 106689. http://dx.doi.org/10.1016/j.aap.2022.106689, URL: https://linkinghub.elsevier.com/retrieve/pii/S0001457522001257.

Yao, Z., Wu, Y., Jiang, Y., Ran, B., 2023. Modeling the fundamental diagram of mixed traffic flow with dedicated lanes for connected automated vehicles. IEEE Trans. Intell. Transp. Syst. 24 (6), 6517–6529. http://dx.doi.org/10.1109/TITS.2022.3219836, URL: https://ieeexplore.ieee.org/document/9965963/.

Yu, H., Jiang, R., He, Z., Zheng, Z., Li, L., Liu, R., Chen, X., 2021. Automated vehicle-involved traffic flow studies: A survey of assumptions, models, speculations, and perspectives. Transp. Res. Part C: Emerg. Technol. 127, 103101. http://dx.doi.org/10.1016/j.trc.2021.103101, URL: https://linkinghub.elsevier.com/retrieve/pii/S0968090X21001224.

Zen, H., Senior, A., 2014. Deep mixture density networks for acoustic modeling in statistical parametric speech synthesis. In: 2014 IEEE International Conference on Acoustics, Speech and Signal Processing. ICASSP, IEEE, pp. 3844–3848. http://dx.doi.org/10.1109/ICASSP.2014.6854321, URL: http://ieeexplore.ieee.org/document/6854321/.

Zhang, J., He, T., Sra, S., Jadbabaie, A., 2019. Why gradient clipping accelerates training: A theoretical justification for adaptivity. In: 8th International Conference on Learning Representations. In: ICLR 2020, URL: http://arxiv.org/abs/1905.11881.

Zhang, H., Liu, Y., Yan, J., Han, S., Li, L., Long, Q., 2020. Improved deep mixture density network for regional wind power probabilistic forecasting. IEEE Trans. Power Syst. 35 (4), 2549–2560. http://dx.doi.org/10.1109/TPWRS.2020.2971607, URL: https://ieeexplore.ieee.org/document/8982039/.

Zhang, X., Sun, J., Sun, J., 2025. On the stochastic fundamental diagram: A general micro-macroscopic traffic flow modeling framework. Commun. Transp. Res. 5, 100163. http://dx.doi.org/10.1016/j.commtr.2025.100163, URL: https://linkinghub.elsevier.com/retrieve/pii/S2772424725000034.

Zhang, X., Sun, J., Zheng, Z., Sun, J., 2024. On the string stability of neural network-based car-following models: A generic analysis framework. Transp. Res. Part C: Emerg. Technol. 160, 104525. http://dx.doi.org/10.1016/j.trc.2024.104525, URL: https://linkinghub.elsevier.com/retrieve/pii/S0968090X24000469.

Zhao, P., Wong, Y.D., Zhu, F., 2024. Modeling the clustering strength of connected autonomous vehicles and its impact on mixed traffic capacity. Commun. Transp. Res. 4, 100151. http://dx.doi.org/10.1016/j.commtr.2024.100151, URL: https://linkinghub.elsevier.com/retrieve/pii/S2772424724000349.

Zhong, X., Zhou, Y., Ahn, S., Chen, D., 2024. Understanding heterogeneity of automated vehicles and its traffic-level impact: A stochastic behavioral perspective. Transp. Res. Part C: Emerg. Technol. 164, 104667. http://dx.doi.org/10.1016/J.TRC.2024.104667.

Zhou, J., Zhu, F., 2020. Modeling the fundamental diagram of mixed human-driven and connected automated vehicles. Transp. Res. Part C: Emerg. Technol. 115, 102614. http://dx.doi.org/10.1016/j.trc.2020.102614, URL: https://linkinghub.elsevier.com/retrieve/pii/S0968090X19313543.